

1 **Title:** Neuromodulation due to propofol affects anesthetic oscillatory coupling

2 **Authors:** Austin E. Soplat^{1,2,3}, Michelle M. McCarthy², Elie M. Adam², Patrick L. Purdon³,

3 Emery N. Brown^{3,4,5}, Nancy Kopell²

4 **Affiliations:**

5 1. Graduate Program for Neuroscience, Boston University, Boston, MA, USA

6 2. Department of Mathematics & Statistics, Boston University, Boston, MA, USA

7 3. Department of Anesthesia, Critical Care and Pain Medicine, Massachusetts General Hospital,

8 Harvard Medical School, Boston, MA, USA

9 4. Department of Brain and Cognitive Sciences, Massachusetts Institute of Technology,

10 Cambridge, MA, USA

11 5. Institute for Medical Engineering and Science, Massachusetts Institute of Technology,

12 Cambridge, MA, USA

13 **Contributions:**

14 Austin E. Soplat: Conceptualization, Data curation, Investigation, Methodology, Software,

15 Analysis, Validation, Visualization, Writing, Editing. Michelle M. McCarthy: Conceptualization,

16 Analysis, Writing, Editing. Elie M. Adam: Software, Visualization, Analysis, Editing. Patrick .

17 Purdon: Funding acquisition, Data curation, Project administration, Supervision, Editing. Emery

18 N. Brown: Funding acquisition, Project administration, Supervision, Editing. Nancy Kopell:

19 Conceptualization, Analysis, Funding acquisition, Project administration, Supervision, Writing,

20 Editing.

21 **Running Head:** Neuromodulation due to propofol affects anes. osc. coupling

22 **Key Words:** anesthesia, thalamocortical oscillations, oscillatory coupling, propofol, thalamus

23

24 **Abstract**

25 The anesthetic propofol produces prominent oscillatory signatures on the EEG. Despite the
26 strong correlation between oscillations and the anesthetic state, the fundamental mechanisms of
27 this unconsciousness remain unknown. On the EEG, propofol elicits alpha oscillations (8-14 Hz),
28 slow oscillations (0.5-2.0 Hz), and dose-dependent phase-amplitude coupling (PAC) between
29 these rhythms. A low enough dose causes “trough-max” PAC, where alpha oscillation amplitude
30 is consistently maximal during slow troughs; this occurs at the same time as arousable
31 unconsciousness. A high enough dose causes consistent “peak-max” PAC, where alpha
32 amplitude is maximal during the slow peak, at the same time asunarousable unconsciousness.
33 Much of the anesthetic state is dominated by a mixture of both states. Using thalamocortical
34 Hodgkin-Huxley simulations, we show that, in addition to propofol effects on GABA_A synapses
35 and thalamocortical H-currents, propofol-induced changes to neuromodulation may generate
36 LFP oscillations and their dose-dependent coupling. We show this for acetylcholine specifically,
37 though other neuromodulators may produce the same effects. We find that LFP- and EEG-
38 relevant synapses of local thalamocortical circuits stochastically display either trough-max or
39 peak-max PAC on any given slow cycle. Trough-max PAC signals are present only in
40 thalamocortical synaptic currents, and not identifiable via membrane potentials alone. PAC
41 preference depends critically on the neuromodulatory state, which is dose-dependent: high doses
42 are associated with statistically more peak-max than trough-max, and vice-versa. This is caused
43 by increased cortical synchronization at higher doses. Our results have important consequences
44 for analyzing LFP/EEG data, in that local network trough- or peak-max may only be seen on a
45 cycle-by-cycle basis, and not when averaging. We hypothesize that this increased cortical

46 synchronization leads to an inability to process signals in a flexible manner needed for awake
47 cognition.

48

49 **New & Noteworthy**

50 We simulate biophysical neural networks to investigate how the anesthetic propofol enables
51 alpha and slow oscillations to emerge and interact. Direct effects of propofol on inhibition and
52 indirect effects on acetylcholine level are necessary for dose-dependent emergence and coupling
53 of these rhythms. Local groups of anesthetized cells behave with more complexity than global
54 EEG would suggest. Higher doses are associated with more cortical synchrony, which may
55 underlie the reduced ability to respond to stimuli.

56

57 **Introduction**

58 Reversible loss of consciousness is the primary aim of all anesthetic agents. Loss of
59 consciousness with the anesthetic propofol is dose-dependent, with lower doses of propofol
60 leading to limited, “arousable” unconsciousness (Purdon et al. 2013; Mukamel et al. 2014;
61 Stephen et al. 2020; Gaskell et al. 2017). For example, with lower doses of propofol, subjects
62 may display decreased arousal but retain their ability to respond to auditory cues if a painful
63 stimulus is applied (Gaskell et al. 2017), or slowly lose their ability to respond (Purdon et al.
64 2013; Mukamel et al. 2014). In contrast, high-dose propofol administration anesthetizes patients
65 into deep, “unarousable” unconsciousness (Purdon et al. 2013; Mukamel et al. 2014; Gaskell et
66 al. 2017; Stephen et al. 2020).

67

68 The EEG during propofol anesthesia is dominated by slow (0.5-2.0 Hz) and alpha (8-14 Hz)
69 oscillations (Purdon et al. 2013; Mukamel et al. 2014). Studies suggest that phase-amplitude
70 coupling (PAC) between slow and alpha oscillations may be an indicator of depth of anesthesia
71 (Purdon et al. 2013; Mukamel et al. 2014). At a sufficiently low dose of propofol, alpha
72 amplitude is maximal during the trough of the slow phase, creating “trough-max” PAC. In
73 contrast, at sufficiently high doses of propofol, alpha amplitude is maximal during the peak of
74 the slow phase, creating “peak-max” PAC (Mukamel et al. 2014). However, large periods of
75 time under propofol do not correspond to either of those states on the temporal scale of
76 spectrogram analysis, instead displaying indeterminant PAC.

77

78 In this computational modeling paper, we show that the notions of alpha-slow trough-max and
79 peak-max PAC exist on the fine timescale of single slow periods locally in space. In local
80 networks, each slow period can exhibit either trough- or peak-max randomly changing in time
81 during the same simulation. We also show that the statistics of these changes are dose-dependent,
82 with higher doses of propofol corresponding to a larger percentage of peak-max rather than
83 trough-max cycles. An important finding of the work is that the statistics of the two PAC states
84 were strongly influenced by the synchrony of the cortical cells. Thus, the depth of anesthesia,
85 measured over a long timescale, corresponds to the statistics of trough- and peak-max states, not
86 a global switch between one state and the other.

87

88 We base our model on previous models suggesting thalamocortical involvement in the
89 production of propofol slow and alpha oscillations and their coupling (Sopkova et al. 2017). Our
90 previous model treated the cortical dynamics strictly as inputs to the thalamic dynamics. Here,

91 we use a full thalamocortical model with feedforward and feedback connections, and the results
92 depend on these connections. Our thalamic model is derived from (Sopkata et al. 2017) and our
93 slow-oscillation-producing cortical model is built on (Compte et al. 2003) (for justification of
94 this cortical slow model, see Methods). The thalamus-to-cortex connections play a prominent
95 role in the synchronization of cortical spiking, which promotes the transition to peak-max.

96

97 Our model includes both direct and indirect effects of propofol: The direct effects are those that
98 affect GABA_A inhibition and thalamocortical cell (TC) H-current, while the indirect effects are
99 from its effects on neuromodulation. We focus on acetylcholine (ACh), which propofol is known
100 to decrease (Kikuchi et al. 1998; Meuret et al. 2000; Nemoto et al. 2013; Pal and Mashour 2021;
101 Luo et al. 2020). In the model, ACh affects several currents, but we find that the essential change
102 is the increase in thalamocortical synaptic strength. ACh-mediated increases in thalamocortical
103 synaptic strength lead to greater cortical synchrony and a statistical shift in the proportion of
104 cycles in trough-max versus peak-max. Other neuromodulators may also be involved, especially
105 those that affect thalamocortical strength.

106

107 **Results**

108

109 **Modeling Objectives and Model Description**

110

111 The aim of our modeling is to explain the dynamic mechanisms underlying the changing PAC
112 seen in experimental data during a large proportion of the anesthetic state under propofol, as
113 illustrated in Figure 1 from approximately time 0 to 45 minutes. Prominent alpha and slow

114 oscillations appear in the EEG of patients under propofol, as shown in Figure 1 A and B. The
115 PAC between alpha and slow changes over time as the dose is increased. Except for very high
116 doses, the PAC is neither wholly trough-max nor wholly peak-max, as shown in Figure 1 B and
117 D. As we will show, our model reproduces alpha and slow frequencies as well as the mix of
118 trough-max and peak-max.

119

120 Our network is composed of 20 Hodgkin-Huxley-type thalamocortical cells (TC), 20 thalamic
121 reticular neurons (TRN), 100 cortical pyramidal soma cell compartments (PYso), 100 cortical
122 pyramidal dendritic cell compartments (PYdr), and 20 cortical interneurons (IN), as illustrated in
123 Figure 2 A (see Methods). We model the effects of propofol by “direct” and “indirect” effects.
124 The direct effects are: increasing GABA_A maximal conductance (\bar{g}_{GABA_A}) and GABA_A decay
125 time constant (τ_{GABA_A}) and decreasing TC cell H-current maximal conductance (\bar{g}_H) (see
126 Methods) (Sopkota et al. 2017). In addition, we model some indirect effects of propofol on
127 neuromodulation, in particular cholinergic modulation, which is known to decrease in the
128 presence of propofol (see Methods and next section) (Kikuchi et al. 1998; Nemoto et al. 2013;
129 Meuret et al. 2000; Pal and Mashour 2021; Luo et al. 2020). The indirect effects are increased
130 intracortical AMPAergic synaptic conductances ($\bar{g}_{AMPA:PY \rightarrow PY}$), TC-to-PY thalamocortical
131 AMPAergic synaptic conductances ($\bar{g}_{AMPA:TC \rightarrow PY}$), and K(Na)-current maximal conductance
132 ($\bar{g}_{K(Na)}$) (see Methods for detail). As we will see, the most important cholinergic effect is the
133 increase in strength of the thalamocortical connections; we hypothesize that other modulators
134 that produce this effect could also produce the same results as in our model. The number of cells
135 in the model is relatively small and is intended to model local activity similar to an LFP signal.

136 The LFP of the model is produced by two sets of synapses: thalamocortical (TC→PY) and
137 intracortical (PY→PY), both targeting the dendrites of cortical pyramidal cells (see Methods).

138

139 The parameters were chosen such that in a baseline condition without propofol, the model
140 produces a depolarized relay-mode state under weak, constant applied current, as shown in
141 Figure 2 B. This simulation exhibits non-bursting, tonic spiking in both the cortex and thalamus
142 as spikes are relayed between regions. Neither region shows high-activity bursts or long periods
143 of quiescence as one would expect in sleep or anesthetized states. This baseline simulation does
144 not exhibit either slow or alpha oscillations spiking.

145

146 **Direct effects do not produce alpha and slow oscillations**

147

148 Our previous work (Sopkova et al. 2017) showed that the "direct" effects of propofol were
149 sufficient for enabling alpha oscillations in a thalamic model with an artificial cortical input. In
150 contrast, our current model expresses neither UP/DOWN slow states nor alpha oscillations in
151 response to the direct effects of propofol across many different values of GABA_A and \bar{g}_H
152 parameter values, as shown in

153

154 Figure 3 A. The lack of DOWN states allows the cortex to continue to send strong, consistent
155 excitation to the anesthetized thalamus, thus interfering with thalamic bursting and propofol
156 alpha oscillations, as shown in

157

158 Figure 3 B and C. More details about this mechanism are in Ancillary Information 1.

159

160 **Neuromodulatory effects enable both alpha and slow oscillations**

161

162 Since direct propofol effects are not able to produce propofol oscillations in our model of the
163 depolarized relay state, we expand our propofol modeling to also include its "indirect" effects.
164 Our indirect effects are modeled as a decrease of cortical ACh in three ways: increasing PY cell
165 K(Na)-current maximal conductance ($\bar{g}_{K(Na)}$) (Compte et al. 2003; Benita et al. 2012), increasing
166 intracortical PY→PY AMPAergic synaptic maximal conductance ($\bar{g}_{AMPA:PY \rightarrow PY}$) (Krishnan et al.
167 2016), and increasing thalamocortical TC→PY AMPAergic synaptic maximal conductance
168 ($\bar{g}_{AMPA:TC \rightarrow PY}$), the latter by way of muscarinic ACh receptors (Kruglikov and Rudy 2008;
169 Favero, Varghese, and Castro-Alamancos 2012).

170

171 With the addition of the indirect effects, the model is able to generate propofol slow and alpha
172 oscillations observed in both the model LFP and the spiking in Figure 4 A and B. The slow
173 oscillation of our cortical model relies on $\bar{g}_{K(Na)}$, as in the sleep slow model from which it was
174 derived (Compte et al. 2003). Random excitation triggers a cortical UP state, during which
175 intracellular sodium builds up, activating the K(Na)-current. This current then terminates the UP
176 state and transitions the pyramidal cells to silent, hyperpolarized DOWN states, just as in the
177 original work (Compte et al. 2003). We assume in our model that these cortical UP and DOWN
178 states correspond, respectively, to the peak and trough of EEG / LFP slow as in natural sleep
179 slow oscillations (Vincenzo Crunelli and Hughes 2010; Cash et al. 2009; Amzica and Steriade
180 2002).

181

182 In addition to slow oscillations, propofol-induced neuromodulation enables thalamic alpha
183 oscillations, as shown in Figure 4. In each slow cycle, the alpha spiking appears in one of two
184 patterns depending on individual slow cycles. During some individual slow cycles, thalamic
185 alpha is present during the cortical DOWN state (blue highlights in Figure 4), while during other
186 slow cycles, thalamic alpha is absent from the cortical DOWN state (orange highlights in Figure
187 4). We refer to the former as trough-max and the latter as peak-max: the two switch apparently
188 randomly on the timescale of seconds, consistent with Figure 1 B. In peak-max, the thalamic
189 alpha exists only in a small range of phases of the slow oscillation. In trough-max, the alpha is
190 spread out over almost the entire slow oscillation cycle, with the most power where cortex is in
191 the DOWN state, making the duration of the alpha longer than in peak-max periods. Though
192 “peak-max” and “trough-max” are defined here in terms of spiking patterns, we will show below
193 that the LFP matches this nomenclature: high alpha in spiking is at the peak of the LFP during
194 peak-max, and high alpha in spiking is around the trough of the LFP during trough-max.

195

196 In the next sections, we will characterize how peak-max and trough-max time periods come
197 about, locally in time in both the spiking and the LFP. For this analysis, we need to understand
198 how the LFP is produced during each of the states by looking at the two kinds of synaptic
199 currents in the model that constitute the LFP: thalamocortical and intracortical synapses that
200 target the pyramidal cell dendrites.

201

202 **Phase-amplitude coupling between alpha and slow oscillations during peak-max**

203

204 During peak-max, thalamic alpha oscillations occur in the spiking only near or during cortical
205 UP states, as shown in Figure 5. Immediately before a cortical UP state, thalamic cells
206 spontaneously burst at the propofol alpha frequency, as shown Figure 5 C. These thalamic bursts
207 initiate a cortical UP state in which the firing is relatively synchronous. The resulting PY→TC
208 depolarization from the synchronous cortical UP is strong enough to depolarize the TC cells into
209 their silent, depolarized state, also known as the “thalamic relay-mode” (see section below
210 “Cortical synchronization modulates thalamic state and is modulated by thalamocortical
211 feedback”). This terminates the thalamic alpha bursting, causing the TC cells to cease oscillating.
212 Loss of TC activity contributes to cessation of cortical spiking and the emergence of the DOWN
213 state. Once both cortical and thalamic cells are quiescent for long enough, the TC cells
214 spontaneously hyperpolarize and initiate bursts again, resetting the cycle.

215

216 We now consider the synaptic currents onto the pyramidal cell dendrites, the constituents
217 currents of the LFP model, during peak-max as shown in Figure 6. During peak-max, both
218 TC→PY and PY→PY synaptic currents are maximal during the cortical UP states, as shown in
219 Figure 4 B and Figure 6. Since thalamic alpha is generated only around the cortical UP, at the
220 peak of the LFP, the coupling between alpha and slow is strong during peak-max, as shown in
221 Figure 4 B, Figure 6 D and Ancillary Information 1. Thus, during peak-max, there is a
222 cooperation in the coupling signal.

223

224 To quantify the amount and preferred slow-phase of alpha power in our LFP signal during this
225 time period, we used the Modulation Index (MI) method (Tort et al. 2010; Purdon et al. 2013) as
226 shown in Figure 7 D. Across the different slow cycles of the combined TC→PY and PY→PY

227 synaptic current comodulogram, the alpha magnitude of the combined synaptic current switches
228 its preference between 0 (middle) on the slow phase, corresponding to the slow peak, and $\pm\pi$
229 (edges), corresponding to the slow trough. During the indicated time period, which corresponds
230 to the orange peak-max time period in 6 A, this current tends towards the slow peak phase
231 instead of the slow trough phase, illustrated by the coupling skewing towards the center. Our
232 simulated peak-max signature highlighted in Figure 7 D is similar to peak-max times in Figure 1
233 of this work.

234

235 **Phase-amplitude coupling between alpha and slow oscillations during trough-max**

236

237 We next examine how the alpha and slow interact during the blue trough-max time periods.
238 During this time, cortical spiking is not tightly synchronized, as shown in Figure 5 A and D. Due
239 to this less synchronized cortical excitation, the thalamus is able to remain hyperpolarized
240 enough during trough-max to have uninterrupted alpha bursting.

241

242 During this trough-max time period, target PYdr compartments exhibit slow oscillations, as
243 shown in Figure 8 B, while the cortically projecting TC cells exhibit alpha oscillations during the
244 cortical DOWN state, as shown in Figure 8 C. The resulting TC \rightarrow PY synaptic current is shown
245 in Figure 8 D. The amplitude of the total TC \rightarrow PY synaptic current fluctuates both with alpha
246 bursts from the thalamus and on a slow timescale due to the fluctuation of the membrane voltage
247 of the PY cells. During cortical slow fluctuations, the synaptic current is maximal during the
248 DOWN/non-spiking (trough) phase of the target cortical cell, as indicated by dashed lines in
249 Figure 8 D and E. This is likely due to the less-synchronous cortex allowing for thalamic alpha to

250 occur for more of the phase than in peak-max. We note that neither the spiking of the TC nor PY
251 cells alone display alpha-slow coupling; the coupling is evident only in the synaptic interaction
252 between the TC cells and the pyramidal cell dendrites.

253

254 In contrast to peak-max, synaptic intracortical currents have very different behavior than
255 synaptic thalamocortical currents during trough-max, as shown in Figure 8 and Figure 9. During
256 peak-max, intracortical currents are maximal during the slow peak or UP state (Figure 8 F-H),
257 whereas thalamocortical currents are maximal during the slow trough or DOWN state (Figure 8
258 B-E). Despite these synaptic currents competing with each other (Figure 9 A and B), the
259 thalamocortical current is an order of magnitude stronger than the intracortical current (Figure 9
260 C), causing the combination of these currents to exhibit trough-max (Figure 9 D).

261

262 **Cortical synchronization modulates thalamic state and is modulated by thalamocortical
263 feedback**

264

265 There are two obvious dynamic differences between trough-max and peak-max: the latter
266 displays more cortical synchronization and the thalamus undergoes periods of silence similar to
267 cortical DOWN states, as shown in Figure 5 and Figure 10. These two phenomena are causally
268 related: during peak-max, the cortical cells are highly synchronized, giving more excitation to
269 the thalamus during the cortical UP state, which depolarizes the thalamus out of its alpha
270 bursting mode into silent depolarization, producing a DOWN state in thalamus. In the absence of
271 cortical synchrony, the thalamus remains more hyperpolarized, producing continuous alpha
272 during cortical DOWN states. Furthermore, in peak-max, the existence of the thalamic DOWN
273 state implies that the cortex receives less excitation during that period, causing the cortex to fire

274 more synchronously during the next UP, since PY cells have not been made to prematurely fire.
275 Thus, there is a reciprocal relationship between spiking synchrony in the cortex and the decrease
276 of alpha in the thalamus.

277

278 The level of cortical synchrony of a slow cycle is produced not only by thalamocortical feedback
279 but also by a stochastic process determined by many factors. These other factors allow switches
280 between peak-max and trough-max on a slow cycle-by-cycle basis. In particular, there is a
281 seemingly chaotic response to similar but different initial conditions: different simulations
282 express very different proportions of time spent in trough-max or peak-max (low or high
283 synchrony). We hypothesize that variables associated with activity of pyramidal cells in the
284 peak-max cortical DOWN state, in which a few pyramidal cells always remain spiking,
285 contribute to the switch from peak-max to trough-max. However, obtaining a complete
286 understanding of the slow cycle-to-cycle variations is outside the scope of this work.

287

288 **Neuromodulation can change preferred PAC regime via changing thalamocortical
289 feedback**

290

291 By modeling higher dose propofol via increasing the indirect effects of ACh, we find that the
292 network shifted from preferring trough-max to peak-max, as shown in Figure 11. To show this,
293 we ran 200 simulations with the previous parameters and random initial conditions, and 200
294 more simulations with the same parameters, except for increases in $\bar{g}_{\text{AMPA:TC} \rightarrow \text{PY}}$, $\bar{g}_{\text{AMPA:PY} \rightarrow \text{PY}}$,
295 and $\bar{g}_{\text{K(Na)}}$, which model further increases in propofol via a decrease in cholinergic modulation.
296 We then averaged the amount of time each simulation exhibited trough-max (data in

297 Supplementary Data 1), since any time not spent in trough-max exhibited peak-max. The lower
298 dose propofol simulations show a slight preference for trough-max over peak-max, with 53% of
299 the time spent in trough-max. In high-dose simulations, the system shifts to a clear preference for
300 peak-max, with trough-max occurring only 27% of the time. There is a high degree of variability
301 among individual simulations, with the proportion of time spent in trough-max having a standard
302 deviation of 20% in the low-dose case and 13% in the high-dose case.

303

304 To understand the cause of this PAC preference shift, we examined each of the propofol indirect
305 effects individually. Starting with low-dose parameters, we changed one indirect effect
306 parameter at a time (i.e., $\bar{g}_{\text{AMPA:TC} \rightarrow \text{PY}}$, $\bar{g}_{\text{AMPA:PY} \rightarrow \text{PY}}$, or $\bar{g}_{\text{K(Na)}}$) and ran 200 more simulations
307 each. With a high dose level of $\bar{g}_{\text{AMPA:TC} \rightarrow \text{PY}}$, the proportion of time spent in trough-max
308 decreases to 30% ($\pm 13\%$), similar to the decrease from low-dose to high-dose propofol with all
309 indirect effects increased. In contrast, with a high-dose level of $\bar{g}_{\text{AMPA:PY} \rightarrow \text{PY}}$ or $\bar{g}_{\text{K(Na)}}$, the
310 proportion of time spent in trough-max is 50% ($\pm 19\%$) or 54% ($\pm 18\%$), respectively. This
311 strongly suggests that changes to thalamocortical synaptic strength are the primary cause of the
312 change in preferred PAC in our model (parameters in Methods and Appendix, data in
313 Supplemental Data 1).

314

315 The shift to peak-max when $\bar{g}_{\text{AMPA:TC} \rightarrow \text{PY}}$ increases is likely due to the increased ability of
316 thalamic bursting to recruit more cortical cells into the synchronized cortical UP state. These
317 synchronized cortical cells send more feedback excitation to TC cells, causing them to enter their
318 depolarized silent state and begin the mutually-enforcing patterns of thalamocortical and
319 corticothalamic interactions that characterize peak max.

320

321 **Discussion**

322

323 **Overview**

324

325 In this work, we simulate a thalamocortical network of Hodgkin-Huxley cells to understand the
326 propofol anesthetic state during which neither trough-max nor peak-max appears to dominate the
327 EEG, though the statistics of these two states change with dose. We find that both the direct
328 effects of propofol on cellular membrane and inhibitory dynamics as well as the indirect effects
329 of propofol mediated by ACh are necessary for producing slow oscillations, alpha oscillation,
330 and their coupling. Slow oscillations generated by cortex and alpha oscillations generated by
331 thalamus couple during propofol states, but do not form stable, long-lasting PAC regimes at the
332 LFP level. The alpha-slow PAC can change from slow cycle to slow cycle in a manner that
333 appeared to be stochastic, with a slight preference for trough-max with a lower dose and a strong
334 preference for peak-max at a higher dose. We found the PAC type distribution depends on the
335 synchronization of the cortex and, therefore, the cortical signal given to the thalamus. At the
336 higher dose of propofol, the increase in $\bar{g}_{\text{AMPA:TC} \rightarrow \text{PY}}$, an indirect effect of propofol due to ACh, is
337 highly influential in changing the preferred PAC type in favor of peak-max. Increasing
338 $\bar{g}_{\text{AMPA:TC} \rightarrow \text{PY}}$ leads to higher synchronization of the cortical pyramidal cells, which leads to
339 stronger and more focused feedback to the thalamus.

340

341 **Prior work and thalamocortical feedback**

342

343 While prior modeling demonstrated thalamocortical circuits could produce propofol alpha
344 oscillations (Ching et al. 2010; Vijayan et al. 2013), or propofol alpha and slow (Krishnan et al.
345 2016), our previous work (Soplat et al. 2017) was the first modeling investigation into the
346 unique alpha-slow PAC dynamics of propofol of which we are aware. Our current
347 thalamocortical model includes feedback from thalamus to cortex, leading to updates of several
348 predictions pertaining to propofol alpha-slow PAC as well as to new mechanistic insights into
349 the role of thalamocortical feedback in network dynamics related to loss of consciousness.

350

351 Our prior model predicted propofol-alpha generation in thalamus due to the direct effects of
352 propofol. Our current thalamocortical model supports thalamic generation of alpha but
353 additionally requires the indirect effect of propofol lowering ACh and decreasing cortical firing
354 to generate this alpha. In the prior thalamus-only model, thalamic alpha emerged only during the
355 DOWN state in trough-max and only during the UP state in peak-max. In the current model, in
356 which the hyperpolarization level of the thalamus is partially controlled by the cortex, we find
357 that, during trough-max, the thalamus does not hyperpolarize enough to stop spiking during the
358 UP state; rather, the thalamus continues to burst in alpha in both cortical UP and DOWN states.
359 We also find that, during peak-max, the thalamic silence during the DOWN state is due to
360 depolarization from corticothalamic excitation, rather than hyperpolarization as suggested by the
361 thalamus-only model. The natural switching between trough-max and peak-max found in the
362 current model relies on thalamocortical feedback, in the shape of partial control of cortical
363 dynamics by the thalamus not available in the prior model.

364

365 Additionally, cortical synchronization, which requires thalamocortical feedback, plays a key role

366 in determining the PAC regime. However, ultimately the PAC regime expressed in each slow
367 cycle is a product of many factors including randomness, and it is outside the scope of this work
368 to evaluate all the determinants of peak-max versus trough-max LFP PAC. Many synaptic and
369 intrinsic factors across different regions could have strong effects on the network dynamics.
370 Even small perturbations to the initial conditions result in radically different simulations,
371 indicating chaotic outcomes in the time course of our simulated LFP PAC. This is similar to the
372 slow oscillations in natural sleep, in that different components of the sleep slow oscillation arise
373 out of different, possibly complementary mechanisms rather than any single set (Neske 2016).

374

375 **Detectability of cycle-by-cycle PAC**

376

377 In Figure 1 it is surprising that we see cycle by cycle changes in EEG experiments. The EEG
378 may be considered to be an average of many LFP signals (Nunez and Srinivasan 2006);
379 therefore, one might expect that cycle-by-cycle LFP PAC changes could be washed out by the
380 EEG spatial averaging. The fact that we do see cycle-by-cycle changes suggests that there may
381 be significant synchrony locally around each EEG electrode.

382

383 If we are correct that TC→PY synapses are the main contributor to the LFP during trough-max,
384 this PAC may not be observable from individual, cortical, or thalamic cell voltages or spike
385 recordings alone. Instead, the EEG signature of trough-max may arise exclusively from
386 TC→PY-generated synaptic current dipoles within the dendrites of pyramidal cells. Therefore,
387 trough-max may appear in cortical electric field measures or spike-field coherence between

388 thalamic spikes and cortical fields, but possibly not spike-field coherence between cortical spikes
389 and cortical fields.

390

391 **Spatiotemporal heterogeneity and future modeling**

392

393

394 Heterogeneity in TC→PY and PY→PY strength and connectivity across cortical regions and
395 layers may contribute to diversity in cortical synchronization levels (Redinbaugh et al. 2020;
396 Malekmohammadi et al. 2019) and therefore diversity in local PAC. Our simulations indicate
397 that different doses of propofol tend to express different PAC regimes on a small spatial scale.
398 Our results also suggest that under propofol, different local cortical networks may, on a fast
399 timescale, switch between trough-max or peak-max at the LFP level in the cortex even while a
400 regional EEG signal predominantly shows a single type of dose-dependent PAC. Our model
401 suggests that during high-dose propofol when the comodulogram predominantly expresses EEG
402 peak-max, the EEG can still exhibit some trough-max PAC cycles, as we see in Figure 1 B.

403

404 By introducing region-specific heterogeneity to cortex (e.g., sensory and higher-order) and
405 thalamus (e.g., core and matrix), future simulations may be able to investigate the significant
406 spatiotemporal changes between low- and high-dose propofol. “Anteriorization” is a well-known
407 phenomenon where propofol administration initially leads to the loss of awake, occipital alpha
408 and an increase in frontal alpha (Tinker, Sharbrough, and Michenfelder 1977; Cimenser et al.
409 2011; Vijayan et al. 2013). This frontal alpha is at its strongest and most persistent state during
410 low-dose EEG trough-max, before spreading to become region-nonspecific during high-dose

411 EEG peak-max PAC (Cimenser et al. 2011; Purdon et al. 2013; Mukamel et al. 2014; Stephen et
412 al. 2020) and decreasing in power with increasing dose (Gutiérrez et al. 2022). Slow power is
413 also greater during high-dose than low-dose propofol (Purdon et al. 2013; Mukamel et al. 2014;
414 Mhuircheartaigh et al. 2013; Lee et al. 2017) and may modulate higher frequencies more in
415 frontal regions during peak-max (Stephen et al. 2020). Modeling prefrontal cortex specifically
416 will allow us to probe why trough-max is prevalent in frontal cortex (Mukamel et al. 2014), why
417 there is stronger frontal slow modulation during peak-max (Stephen et al. 2020), and why there
418 is increased thalamocortical alpha coherence in this region (Flores et al. 2017). Simultaneously
419 modeling of sensory cortex will allow us to explore coherence, phase (Malekmohammadi et al.
420 2019), and firing rate (Krom et al. 2020) discrepancies found between frontal and sensory
421 regions under anesthesia. Understanding how heterogeneity affects cross-cortical communication
422 and frontal cortex specifically may help to validate theories of loss of consciousness, including
423 frontoparietal disconnection (Hudetz and Mashour 2016) and similar connectivity changes
424 (Banks et al. 2020), brainstem changes to neuromodulation (Brown, Purdon, and Van Dort
425 2011), alpha blocking of processing (Palva and Palva 2007), and slow oscillation control of
426 activity (Gemignani et al. 2015; Stephen et al. 2020).

427

428 **Propofol, slow oscillations, and neuromodulation**

429

430 A notable interpretation of this model is that the anesthetic effects depend on the indirect
431 neuromodulatory effects of ACh as much as on the direct effects on GABA_A inhibition and the
432 TC cell H-currents; however, any other modulator that increases the strength of coupling from
433 thalamus to cortex will likely have the same effect. While we restrict our investigation here to

434 propofol cholinergic changes, propofol likely also utilizes known slow mechanisms via its
435 effects on non-cholinergic brainstem neuromodulatory systems. Propofol affects not just the
436 cholinergic sources in the basal forebrain, laterodorsal tegmental area, and pedunculopontine
437 tegmental area, but, through enhancing inhibition by the pre-optic area, also inhibits the
438 tuberomammillary nucleus, locus coeruleus, dorsal raphe nucleus, ventral periaqueductal gray,
439 and lateral hypothalamus (Brown, Lydic, and Schiff 2010; Brown, Purdon, and Van Dort 2011).
440 These areas respectively provide histamine, norepinephrine, serotonin, dopamine, and
441 orexin/hypocretin to the cortex (Brown, Lydic, and Schiff 2010; Brown, Purdon, and Van Dort
442 2011). Many of these neuromodulators affect various potassium currents that are critical in
443 known slow models, including the K(Na)-current, the NaP-current, and potassium leak currents
444 (Schwindt, Spain, and Crill 1989; McCormick 1992). These neuromodulators can also affect
445 both excitatory and inhibitory currents in the cortex, and can change the relative impact of
446 thalamocortical synapses (McCormick 1992; Favero, Varghese, and Castro-Alamancos 2012;
447 Kuo and Dringenberg 2008). However, there is still much we do not understand about how these
448 neuromodulators work in concert together (Krishnan et al. 2016). Global GABA_A conductance
449 strength, which is very important in the mechanisms of propofol, has also been found to vary
450 across natural sleep and has been analyzed alongside other neuromodulators in a similar
451 thalamocortical model (Krishnan et al. 2016). Additionally, increasing K(Na) strength decreases
452 the frequency of slow oscillations in this cortical model (Benita et al. 2012), and this current
453 behaves similarly to ATP-dependent K-currents previously used in burst suppression modeling
454 (Cunningham et al. 2006, 200; Ching et al. 2012). Therefore, by further exploring the slow
455 oscillation mechanism in this work and including slow mechanisms impacted by non-cholinergic

456 and metabolic neuromodulators, it may be possible to augment this model to simulate not just
457 propofol PAC regimes, but also burst suppression.

458

459 It is known that the cholinesterase inhibitor physostigmine reverses propofol LOC (Meuret et al.
460 2000); assuming LOC depends on slow oscillations, our model suggests that the indirect
461 engagement of the K(Na) current by propofol may explain this experimental result.

462 Physostigmine acts to increase ACh levels, which would decrease $\bar{g}_{K(Na)}$ in our model and stop
463 the K(Na)-dependent slow, thus eliminating propofol-induced slow. ACh also acts to weaken
464 thalamocortical connections (Favero, Varghese, and Castro-Alamancos 2012) and therefore
465 release the cortex from over-synchronization; less synchronized states are associated with the
466 awake state. Thus, loss of ACh may be a major contributor to propofol-induced loss of
467 consciousness. The fact that our model requires neuromodulatory changes to produce propofol
468 oscillations and their coupling suggests that the effects of propofol on the brainstem may be
469 critical for its oscillatory phenomena, which is supported by active experimental research on
470 propofol and other anesthetics (Moody et al. 2021; Minert, Yatziv, and Devor 2017; Minert,
471 Baron, and Devor 2020; Muindi et al. 2016; Vlasov et al. 2021). Since the transition from
472 trough-max to peak-max is associated with only lowering ACh in our model, we predict that a
473 smaller dose of physostigmine may promote less peak-max.

474

475 In addition to a deeper understanding of the role of ACh in the dynamics of anesthesia, our
476 model makes predictions about effects of localized injections of propofol and ACh receptor
477 antagonist, scopolamine. If propofol is locally injected into the thalamus, and scopolamine is
478 locally injected into the cortex, we predict that propofol slow and alpha oscillations would

479 appear on the EEG. This would happen due to the cortical decrease in ACh, enabling K(Na)-
480 current activation, thus generating cortical slow, which in combination with the direct effects of
481 propofol in thalamus would enable thalamic alpha. Different doses of scopolamine in this case
482 may be able to induce predominantly EEG trough-max or peak-max as well, depending on how
483 ACh modulation through scopolamine affects thalamocortical synaptic strength.

484

485 **Propofol, slow oscillations, and sleep**

486

487 Our work suggests that propofol utilizes not only thalamic spindling mechanisms (Soplata et al.
488 2017), but also natural sleep slow mechanisms and changes in neuromodulation to produce its
489 oscillatory and PAC effects. The K(Na)-current is the primary mechanism of slow generation in
490 the cortical sleep slow model we used (Sanchez-Vives, Nowak, and McCormick 2000; Schwindt,
491 Spain, and Crill 1989; Compte et al. 2003). Because propofol decreases ACh in the cortex
492 (Kikuchi et al. 1998; Nemoto et al. 2013), and decreasing ACh strengthens the K(Na)-current
493 (Schwindt, Spain, and Crill 1989; McCormick 1992) (see Introduction), indirect cholinergic
494 effects by propofol on this current may contribute to propofol slow generation. Most other slow
495 models rely on a combination of changes to cortical excitatory/inhibitory plasticity and/or the
496 persistent sodium current (NaP) (Bazhenov et al. 2002; Hill and Tononi, Giulio 2004; V.
497 Crunelli et al. 2011; Sanchez-Vives and McCormick 2000; Timofeev et al. 2000; Krishnan et al.
498 2016). The NaP-current has been shown to be functionally coupled to the K(Na)-current (Hage
499 and Salkoff 2012), and therefore the K(Na)-current may contribute to these mechanisms. Models
500 of slow UP state initiation, also called DOWN-to-UP transitions, rely on random cortical
501 excitation (Timofeev et al. 2000), synaptic plasticity changes (Krishnan et al. 2016; Sanchez-

502 Vives and McCormick 2000), or TC initiation of cortical slow UP states (V. Crunelli et al. 2011).
503 In our trough-max simulations, persistent thalamic alpha provides constant excitation relative to
504 cortical slow oscillations, enabling UP states to initiate as soon as the hyperpolarizing K(Na)-
505 current in a PY cell has decayed. In our peak-max simulations, however, TC cells exhibit their
506 own silent depolarized states, and upon thalamic re-hyperpolarization, sudden intrinsic thalamic
507 bursting onto a silent cortex enables synchronized cortical UP states. Future work designed to
508 differentiate natural sleep slow versus anesthetic slow mechanisms will enable finer-grained
509 experiments into how the loss of consciousness occurs in these two distinct states.

510

511 **Propofol, memory consolidation, and aging**

512

513 Our investigation of these thalamocortical dynamics under propofol may have implications for
514 memory and aging. During natural sleep, memory consolidation onto cortical axo-dendrite
515 connections likely occurs during the nesting of hippocampal ripples during thalamic spindles,
516 which themselves are nested inside thalamocortical sleep slow oscillations (Penagos, Varela, and
517 Wilson 2017). Based on our current and previous work (Soplatá et al. 2017), propofol alpha and
518 slow oscillations likely utilize some of the same mechanisms used by these processes. Proper
519 memory consolidation requires correct encoding of worthwhile memories during sleep
520 (Stickgold 2005), but if application of propofol abnormally activates some of the same
521 oscillations in this process, the oscillations of propofol may cause invalid memory consolidation
522 or interfere with synaptic-dendrite networks involved in storing memory. A recent experiment
523 showed promising results in using propofol to disrupt reconsolidation of traumatic memories
524 (Galarza Vallejo et al. 2019), which could help treat Post-Traumatic Stress Disorder patients.

525 Additionally, alpha power and, to a lesser extent, slow power under propofol may indicate a
526 subject's "brain age" (Purdon et al. 2015). Our modeling predicts that propofol alpha may
527 exclusively arise from the thalamus, and therefore a decrease in propofol alpha power across age
528 could correlate with brain fitness via losses in the ability of the thalamus to burst (Purdon et al.
529 2015), myelination retention of thalamocortical afferents (Peters 2002), or the strength of
530 thalamocortical synapses onto cortical dendrites (Morrison and Baxter 2012).

531

532 **Implications for unconsciousness**

533

534 One unintuitive finding suggested by our model was that TC neurons may be depolarized into
535 "relay mode" during peak-max DOWN states, and could potentially relay sensory information
536 during this window, even during anesthesia. In our simulations, strong corticothalamic excitation
537 after synchronized UP states increased the membrane potential of TC cells during peak-max, as
538 shown in Figure 6. This increase was enough to interrupt the intrinsic alpha bursts of the
539 thalamus, but if this occurs at the same time as strong sensory input spikes, the TC cells may be
540 depolarized enough to briefly relay sensory spiking information up to the cortex. Recently, in
541 humans under low propofol anesthesia, auditory stimuli resulted in wake-like cortical neural
542 activity in primary auditory cortex but not higher-order cortex (Krom et al. 2020). This suggests
543 that some thalamic sensory relay may still occur under propofol anesthesia, even if changes to
544 cross-cortical communication prevent its higher-order processing. Furthermore, in our
545 simulations, peak-max may occur during individual slow cycles of both low- and high-dose
546 propofol, indicating this brief sensory relay may occur at any point during propofol anesthesia
547 (Malekmohammadi et al. 2019; Krom et al. 2020).

548

549 Our modeling of how propofol alters coordination of thalamocortical oscillatory activity may
550 help explain how anesthesia leads to arousable and unarousable loss of consciousness. While our
551 model of PAC shows how sensory stimuli can still reach primary regions of cortex (see previous
552 paragraph), it also suggests that there may be large dynamic changes in UP state synchrony
553 among cortical neurons. If thalamic bursting is enhanced under propofol, and enhanced
554 thalamocortical feedback can strongly synchronize cortical UP states, then the cortical
555 coordination needed for consciousness may be disrupted by too much synchrony within local
556 cortical networks. Our model suggests that this occurs during peak-max, which happens more
557 frequently at higher doses, and therefore this increase in local LFP-scale synchrony (as opposed
558 to large-scale synchrony) may be responsible for the difference between arousable and
559 unarousable propofol unconsciousness. At the same time, since ACh strengthens $\bar{g}_{\text{AMPA:PY} \rightarrow \text{PY}}$,
560 during high propofol doses, UP state synchrony may be more likely to spread between
561 neighboring cortical columns, which may also explain the shift from arousable to unarousable
562 unconsciousness under propofol. Finally, enhanced intracortical UP state synchrony during peak-
563 max may also explain why peak-max coupling could extend to frequencies higher than alpha
564 (Stephen et al. 2020) if higher frequency activity spreads more easily through these synchronized
565 UP states. Ultimately, our model and the future work it guides may help to find the mechanistic
566 difference between arousable and unarousable unconsciousness and, possibly, one cause of loss
567 of consciousness.

568

569 **Methods**

570

571 *Model Network Design*

572

573 Our Hodgkin-Huxley network, illustrated in Figure 2 A, consists of 100 cortical pyramidal
574 dendritic compartments (PYdr), 100 corresponding cortical pyramidal somatic/axonal
575 compartments (PYso), 20 cortical interneuron cells (INs), 20 thalamic thalamocortical cells
576 (TCs), and 20 thalamic reticular neurons (TRNs). All equations and parameters used in the
577 model are available in both the Appendix and the model code (Soplata 2022b). The thalamic
578 cells are identical to those used in (Soplata et al. 2017) and therefore derived from (Destexhe et
579 al. 1996; Ching et al. 2010), except that we used a population size of 20 for each cell class rather
580 than 50 due to memory/RAM limitations. All intrathalamic synapses between populations are
581 all-to-all connected, just like in (Soplata et al. 2017). The cortical compartments and cells are
582 implemented according to their original description in (Compte et al. 2003). For all cortical and
583 thalamocortical synapses, each source cell is connected to (2*radius+1) target cells, where the
584 radius is 10 cells. These connections overlap at the beginning and end of each cells for each
585 population, and all synapses of a given source cell are equally weighted. Each PYdr
586 compartment is directly coupled to a single corresponding PYso compartment. While there are
587 many slow models to choose from (Lytton, Destexhe, and Sejnowski 1996; Destexhe et al. 1996;
588 Sanchez-Vives and McCormick 2000; Timofeev et al. 2000; Bazhenov et al. 2002; Destexhe and
589 Sejnowski 2003; Hill and Tononi, Giulio 2004; V. Crunelli et al. 2011), we use this particular
590 K(Na)-based sleep slow cortical model (Compte et al. 2003) due to its simplicity, experimental
591 basis (Sanchez-Vives and McCormick 2000), and effective utilization in other slow models
592 (Benita et al. 2012; Taxidis et al. 2013).

593

594 All connections are illustrated in Figure 2 A and available in both the Appendix and the model
595 code (Soplat 2022b). AMPA connections include from PYso to neighbor-only PYdr
596 (PYso→PYdr also called PY→PY), from PYso to IN (PY→IN), from TC to TRN (TC→TRN),
597 from TC to PYdr (TC→PY), from TC to IN (TC→IN), from PYso to TRN (PY→TRN), and
598 from PYso to TC (PY→TC). Intracortical AMPA connections (PYso→PYdr and PYso→IN)
599 included synaptic depression. NMDA connections include from PYso to PYdr and from PYso to
600 IN and include synaptic depression. GABA_A connections include from IN to PYso (IN→PY),
601 from IN to neighbor-only IN (IN→IN), from TRN to TC (TRN→TC), and from TRN to TRN
602 (TRN→TRN). GABA_B connections are only from TRN to TC (TC→TRN). Finally, simple
603 compartmental connections exist between each PYdr and its corresponding PYso compartment.
604 Note that we use PY→PY to refer exclusively to AMPAergic PYso→PYdr connections.
605

606 *Propofol direct effects*

607

608 Similarly to our previous work (Soplat et al. 2017), we model how increasing propofol directly
609 affects the thalamocortical system via changing three parameters: decreasing TC cell H-current
610 maximal conductance (\bar{g}_H), and potentiating all GABA_A synapses via increasing maximal
611 conductance (\bar{g}_{GABA_A}) and GABA_A decay time constants (τ_{GABA_A}). Propofol may decrease \bar{g}_H
612 directly (Ying et al. 2006; Cacheaux et al. 2005), although the magnitude of this change is
613 experimentally unknown (Chen 2005). To shift from a relay-mode state to a propofol-
614 anesthetized state, we decrease \bar{g}_H from 0.04 to 0.005 mS/cm^2 , which is in line with previous
615 anesthetic and sleep research using this thalamic model (Destexhe et al. 1996; Vijayan et al.
616 2013; Ching et al. 2010; Soplat et al. 2017).

617

618 For our propofol simulations, we triple \bar{g}_{GABA_A} and τ_{GABA_A} for all $GABA_A$ synapses, since
619 doubling these $GABA_A$ parameters did not effectively produce trough-max. We originally based
620 the magnitude of our propofol $GABA_A$ changes on prior modeling work (McCarthy, Brown, and
621 Kopell 2008). In our previous paper (Soplat et al. 2017), we found that our thalamus-only
622 network could produce persistent alpha oscillations if we doubled or tripled these $GABA_A$
623 parameters. Importantly, in Figure 4 of (Soplat et al. 2017), we showed that thalamic persistent
624 alpha occurred across a broader range of inputs when tripling the parameters compared to
625 doubling. In the current paper, for all anesthetic simulation variations, doubling $GABA_A$
626 parameters produces very little simulation time of trough-max, instead producing peak-max, due
627 to the lack of persistent thalamic alpha oscillations. Instead, only by tripling $GABA_A$ parameters
628 do the simulations produce trough-max for a substantial or majority of simulation time. We
629 suspect that cortical dynamics with lower doses of propofol require additional cortical cell types
630 such as found in (McCarthy, Brown, and Kopell 2008). Since these cell types were not included
631 in the model, we restrict our examination of cortical dynamics and its effects on thalamus to
632 higher, anesthetic doses of propofol.

633

634 *Propofol indirect effects (acetylcholine)*

635

636 Propofol decreases cortical acetylcholine (ACh) (see Introduction), and we model these
637 “indirect” anesthetic changes via increasing intracortical AMPAergic synaptic conductances
638 ($\bar{g}_{AMPA:PY \rightarrow PY}$) (Compte et al. 2003; Benita et al. 2012; Krishnan et al. 2016), TC-to-PY
639 thalamocortical AMPAergic synaptic conductances ($\bar{g}_{AMPA:TC \rightarrow PY}$) (Kruglikov and Rudy 2008;

640 Favero, Varghese, and Castro-Alamancos 2012), and K(Na)-current maximal conductance
641 ($\bar{g}_{K(Na)}$) (Compte et al. 2003; Benita et al. 2012). ACh affects thalamocortical afferent synapses
642 in different ways: decreased nicotinic ACh receptor activation weakens thalamocortical
643 synapses, but decreased muscarinic ACh receptor activation strengthens them (Kruglikov and
644 Rudy 2008; Favero, Varghese, and Castro-Alamancos 2012; Gil, Connors, and Amitai 1997;
645 Hsieh, Cruikshank, and Metherate 2000; Oldford and Castro-Alamancos 2003; Eggermann and
646 Feldmeyer 2009). Based on the rapid desensitization of nicotinic ACh receptors (Quick and
647 Lester 2002), the slowly-changing, metabotropic nature of muscarinic receptors, and their similar
648 shifts in natural sleep (McCormick 1992), we believe that muscarinic receptors could exert a
649 stronger effect than nicotinic receptors on thalamocortical afferents, therefore increasing
650 $\bar{g}_{AMPA:TC \rightarrow PY}$ with increasing propofol dose.

651

652 *Dose parameters*

653

654 For relay-mode, we apply none of the propofol effects and use the following parameters:
655 $\bar{g}_{AMPA:PY \rightarrow PY}$ 0.004 mS/cm², $\bar{g}_{AMPA:TC \rightarrow PY}$ 0.004 mS/cm², TC \bar{g}_H 0.04 mS/cm², PY $\bar{g}_{K(Na)}$ 0
656 mS/cm², and global \bar{g}_{GABA_A} and τ_{GABA_A} modifier: 1x. We choose our relay-mode TC→PY and
657 PY→PY maximal synaptic conductances (both 0.004 mS/cm²) based on values slightly less
658 than the value needed for one source cell spike to induce one target cell spike.

659

660 For direct-effects-only and all low-dose and high-dose propofol simulations, propofol direct
661 effect parameters are as follows: TC \bar{g}_H 0.005 mS/cm² and global \bar{g}_{GABA_A} and τ_{GABA_A} modifier:
662 3x. We do not change propofol direct effect parameters between low- and high-dose propofol

663 because only tripling rather than doubling GABA_A parameters enabled trough-max (see previous
664 section *Propofol direct effects*) and further changes to \bar{g}_H may have changed the frequency and
665 susceptibility of thalamic alpha when our primary aim was to investigate how thalamic alpha
666 interacts with cortical slow coupling.

667

668 For low-dose propofol simulations, corresponding to indirect effects, we increase PY $\bar{g}_{K(Na)}$ to
669 1.33 mS/cm^2 , $\bar{g}_{\text{AMPA:TC} \rightarrow \text{PY}}$ to 0.005 mS/cm^2 and $\bar{g}_{\text{AMPA:PY} \rightarrow \text{PY}}$ to 0.0075 mS/cm^2 , while for
670 high-dose simulations, we further increase PY $\bar{g}_{K(Na)}$ to 1.5 mS/cm^2 and both $\bar{g}_{\text{AMPA:TC} \rightarrow \text{PY}}$ and
671 $\bar{g}_{\text{AMPA:PY} \rightarrow \text{PY}}$ to 0.01 mS/cm^2 . Low- and high-dose values of PY $\bar{g}_{K(Na)}$ were used for their
672 similarity to slow investigations with the original model (Benita et al. 2012). Different
673 computational models use a range of proportional increases to $\bar{g}_{\text{AMPA:PY} \rightarrow \text{PY}}$ caused by ACh,
674 including up to +75% (Vijayan et al. 2013) or +15% to +100% (Krishnan et al. 2016). Data on
675 how much ACh may increase $\bar{g}_{\text{AMPA:TC} \rightarrow \text{PY}}$ is much more scarce, but the increase may be as high
676 as +300% (see Figure 8 F of (Favero, Varghese, and Castro-Alamancos 2012)). However, the
677 effect of these ACh changes on the system may be even more pronounced due to the large
678 differences in intracortical and thalamocortical maximal AMPAergic conductance assumptions,
679 which can span more than an order of magnitude of difference just between biophysical models
680 alone (Traub et al. 2005; Ching et al. 2010; Vijayan et al. 2013; Krishnan et al. 2016). Based on
681 our initial relay-mode $\bar{g}_{\text{AMPA:PY} \rightarrow \text{PY}}$ and $\bar{g}_{\text{AMPA:TC} \rightarrow \text{PY}}$ values of 0.004 mS/cm^2 , we limit our
682 analysis to the extensive network changes that occur within +150% of these values to try to stay
683 as close to biological realism as possible. The only exception to this is where we increase each
684 indirect effect to its corresponding high-dose level by itself (given above) but kept all other
685 values at low-dose conditions.

686

687 *LFP Model*

688

689 For our LFP model and PAC analysis, we rely on the total combined cortical AMPAergic
690 synaptic currents of TC→PY and PY→PY synapses, in units of $\mu A/cm^2$, except when otherwise
691 indicated to look at individual synapse types. We base this analysis on the assumption that the
692 primary determinants of LFP, like most electrode signals, are local excitatory synaptic currents
693 (Nunez and Srinivasan 2006; Buzsáki, Anastassiou, and Koch 2012; Einevoll et al. 2013).

694

695 *Coupling Analysis*

696

697 For the comodulograms of the LFP signals, we use the Modulation Index method (Tort et al.
698 2010) as implemented in MATLAB by Angela Onslow (Onslow, Bogacz, and Jones 2011) to
699 estimate phase-amplitude coupling in Figure 7 and Figure 9. A copy of this analysis software is
700 available in the modified DynaSim toolbox used for this work (Sopłata 2022a), and the
701 parameters used for each analysis are available online in the script files used to run the
702 simulations and analysis (Sopłata 2022b).

703

704 *Simulations and Reproducibility*

705

706 All of the simulation parameters (Sopłata 2022b) and model code (Sopłata 2022c) needed to
707 reproduce the simulations shown in this work are available online on GitHub. All simulations
708 were run using a custom version (Sopłata 2022a) of the MATLAB simulation toolbox DynaSim

709 (Sherfey et al. 2018) located online. Individual simulations should be reproducible on a modern
710 desktop computer with access to RAM of 32 gigabytes or higher.

711

712 *Human Data for Figure 1*

713

714 Human experimental data used in Figure 1 is from a single subject analyzed in (Purdon et al.
715 2013) and subject to the same methodology and analysis.

716

717 **Appendix:**

718 **Equations for Computational Models (attached as PDF)**

719

720 **Acknowledgements:**

721 The authors would like to thank Jason Sherfey, Erik A. Roberts, and Caroline Moore-Kochlacs
722 for their suggestions during the investigation.

723

724 **Grants:**

725 All authors were supported by NIH Grant P01GM118269. Other sources include Guggenheim
726 Fellowship in Applied Mathematics, NIH R01-GM104948, funds from MGH, and NSF DMS-
727 1042134-5.

728

729 **Disclosures:**

730 Massachusetts General Hospital has licensed intellectual property for EEG monitoring developed
731 by Drs. Brown and Purdon to Masimo Corporation. Drs. Brown and Purdon hold interests in, and

732 Dr. Purdon is a co-founder of, PASACALL Systems, Inc., a start-up company developing EEG-
733 based anesthetic state control systems for anesthesiology.

734

735 **Supplements:**

736 **Supplemental Data 1. Simulation PAC data, available at**

737 <https://doi.org/10.6084/m9.figshare.19175720.v1>

738

739 **Endnote:**

740 At the request of the author(s), readers are herein alerted to the fact that additional materials

741 related to this manuscript (“Ancillary Information 1”) may be found at

742 <https://doi.org/10.6084/m9.figshare.19184564>. These materials are not a part of this manuscript

743 and have not undergone peer review by the American Physiological Society (APS). APS and the

744 journal editors take no responsibility for these materials, for the website address, or for any links

745 to or from it.

746

747 **References**

- 748 Amzica, Florin, and Mircea Steriade. 2002. “The Functional Significance of K-Complexes.”
- 749 *Sleep Medicine Reviews* 6 (2): 139–49. <https://doi.org/10.1053/smrv.2001.0181>.
- 750 Banks, Matthew I., Bryan M. Krause, Christopher M. Endemann, Declan I. Campbell,
- 751 Christopher K. Kovach, Mark Eric Dyken, Hiroto Kawasaki, and Kirill V. Nourski. 2020.
- 752 “Cortical Functional Connectivity Indexes Arousal State during Sleep and Anesthesia.”
- 753 *NeuroImage* 211 (May): 116627. <https://doi.org/10.1016/j.neuroimage.2020.116627>.
- 754 Bazhenov, Maxim, Igor Timofeev, Mircea Steriade, and Terrence J Sejnowski. 2002. “Model of
- 755 Thalamocortical Slow-Wave Sleep Oscillations and Transitions to Activated States.” *The*
- 756 *Journal of Neuroscience* □: The Official Journal of the Society for Neuroscience. 22 (19):
- 757 8691–8704. <https://doi.org/10.1523/JNEUROSCI.22-19-08691.2002>.
- 758 Benita, Jose M., Antoni Guillamon, Gustavo Deco, and Maria V. Sanchez-Vives. 2012.
- 759 “Synaptic Depression and Slow Oscillatory Activity in a Biophysical Network Model of
- 760 the Cerebral Cortex.” *Frontiers in Computational Neuroscience* 6.
- 761 <https://doi.org/10.3389/fncom.2012.00064>.
- 762 Brown, Emery N., Ralph Lydic, and Nicholas D. Schiff. 2010. “General Anesthesia, Sleep, and
- 763 Coma.” *The New England Journal of Medicine* 363 (27): 2638–50.
- 764 <https://doi.org/10.1056/nejmra0808281>.
- 765 Brown, Emery N., Patrick L. Purdon, and Christa J. Van Dort. 2011. “General Anesthesia and
- 766 Altered States of Arousal: A Systems Neuroscience Analysis.” *Annual Review of*
- 767 *Neuroscience* 34 (1): 601–28. <https://doi.org/10.1146/annurev-neuro-060909-153200>.

- 768 Buzsáki, György, Costas A. Anastassiou, and Christof Koch. 2012. “The Origin of Extracellular
769 Fields and Currents — EEG, ECoG, LFP and Spikes.” *Nature Reviews Neuroscience* 13
770 (6): 407–20. <https://doi.org/10.1038/nrn3241>.
- 771 Cacheaux, L. P., Norbert Topf, Gareth R. Tibbs, Ulrich R. Schaefer, Roberto Levi, Neil L.
772 Harrison, Geoffrey W. Abbott, and Peter A. Goldstein. 2005. “Impairment of
773 Hyperpolarization-Activated, Cyclic Nucleotide-Gated Channel Function by the
774 Intravenous General Anesthetic Propofol.” *The Journal of Pharmacology and
775 Experimental Therapeutics* 315 (2): 517–25. <https://doi.org/10.1124/jpet.105.091801>.
- 776 Cash, S. S., E. Halgren, N. Dehghani, A. O. Rossetti, T. Thesen, C. Wang, O. Devinsky, et al.
777 2009. “The Human K-Complex Represents an Isolated Cortical Down-State.” *Science*
778 324 (5930): 1084–87. <https://doi.org/10.1126/science.1169626>.
- 779 Chen, X. 2005. “HCN Subunit-Specific and cAMP-Modulated Effects of Anesthetics on
780 Neuronal Pacemaker Currents.” *Journal of Neuroscience* 25 (24): 5803–14.
781 <https://doi.org/10.1523/JNEUROSCI.1153-05.2005>.
- 782 Ching, S., A. Cimenser, P. L. Purdon, E. N. Brown, and N. J. Kopell. 2010. “Thalamocortical
783 Model for a Propofol-Induced Alpha-Rhythm Associated with Loss of Consciousness.”
784 *Proceedings of the National Academy of Sciences of the United States of America* 107
785 (52): 22665–70. <https://doi.org/10.1073/pnas.1017069108>.
- 786 Ching, S., P. L. Purdon, S. Vijayan, N. J. Kopell, and E. N. Brown. 2012. “A
787 Neurophysiological-Metabolic Model for Burst Suppression.” *Proceedings of the
788 National Academy of Sciences of the United States of America* 109 (8): 3095–3100.
789 <https://doi.org/10.1073/pnas.1121461109>.

- 790 Cimenser, A., P. L. Purdon, E. T. Pierce, J. L. Walsh, A. F. Salazar-Gomez, P. G. Harrell, C.
791 Tavares-Stoeckel, K. Habeeb, and E. N. Brown. 2011. “Tracking Brain States under
792 General Anesthesia by Using Global Coherence Analysis.” *Proceedings of the National
793 Academy of Sciences* 108 (21): 8832–37. <https://doi.org/10.1073/pnas.1017041108>.
- 794 Compte, Albert, Maria V. Sanchez-Vives, David A. McCormick, and Xiao-Jing Wang. 2003.
795 “Cellular and Network Mechanisms of Slow Oscillatory Activity (<1 Hz) and Wave
796 Propagations in a Cortical Network Model.” *Journal of Neurophysiology* 89 (5): 2707–
797 25. <https://doi.org/10.1152/jn.00845.2002>.
- 798 Crunelli, V., A. C. Errington, S. W. Hughes, and T. I. Toth. 2011. “The Thalamic Low-
799 Threshold Ca²⁺ Potential: A Key Determinant of the Local and Global Dynamics of the
800 Slow (<1 Hz) Sleep Oscillation in Thalamocortical Networks.” *Philosophical
801 Transactions of the Royal Society of London. A* 369 (1952): 3820–39.
802 <https://doi.org/10.1098/rsta.2011.0126>.
- 803 Crunelli, Vincenzo, and Stuart W Hughes. 2010. “The Slow (<1 Hz) Rhythm of Non-REM
804 Sleep: A Dialogue between Three Cardinal Oscillators.” *Nature Neuroscience* 13 (1): 9–
805 17. <https://doi.org/10.1038/nn.2445>.
- 806 Cunningham, M. O., D. D. Pervouchine, C. Racca, N. J. Kopell, C. H. Davies, R. S. G. Jones, R.
807 D. Traub, and M. A. Whittington. 2006. “Neuronal Metabolism Governs Cortical
808 Network Response State.” *Proceedings of the National Academy of Sciences* 103 (14):
809 5597–5601.
- 810 Destexhe, Alain, Thierry Bal, David A. McCormick, and Terrence J. Sejnowski. 1996. “Ionic
811 Mechanisms Underlying Synchronized Oscillations and Propagating Waves in a Model

- 812 of Ferret Thalamic Slices.” *Journal of Neurophysiology* 76 (3): 2049–70.
- 813 <https://doi.org/10.1152/jn.1996.76.3.2049>.
- 814 Destexhe, Alain, and T. J. Sejnowski. 2003. “Interactions between Membrane Conductances
- 815 Underlying Thalamocortical Slow-Wave Oscillations.” *Physiological Reviews* 83 (4):
- 816 1401–53. <https://doi.org/10.1152/physrev.00012.2003>.
- 817 Eggermann, Emmanuel, and Dirk Feldmeyer. 2009. “Cholinergic Filtering in the Recurrent
- 818 Excitatory Microcircuit of Cortical Layer 4.” *Proceedings of the National Academy of*
- 819 *Sciences* 106 (28): 11753–58. <https://doi.org/10.1073/pnas.0810062106>.
- 820 Einevoll, Gaute T., Christoph Kayser, Nikos K. Logothetis, and Stefano Panzeri. 2013.
- 821 “Modelling and Analysis of Local Field Potentials for Studying the Function of Cortical
- 822 Circuits.” *Nature Reviews Neuroscience* 14 (11): 770–85.
- 823 <https://doi.org/10.1038/nrn3599>.
- 824 Favero, Morgana, Gladis Varghese, and Manuel A Castro-Alamancos. 2012. “The State of
- 825 Somatosensory Cortex during Neuromodulation.” *Journal of Neurophysiology* 108 (4):
- 826 1010–24. <https://doi.org/10.1152/jn.00256.2012>.
- 827 Flores, Francisco J., Katharine E. Hartnack, Amanda B. Fath, Seong-Eun Kim, Matthew A.
- 828 Wilson, Emery N. Brown, and Patrick L. Purdon. 2017. “Thalamocortical
- 829 Synchronization during Induction and Emergence from Propofol-Induced
- 830 Unconsciousness.” *Proceedings of the National Academy of Sciences of the United States*
- 831 *of America* 114 (32): E6660–68. <https://doi.org/10.1073/pnas.1700148114>.
- 832 Galarza Vallejo, Ana, Marijn C W Kroes, Enrique Rey, Maria Victoria Acedo, Stephan Moratti,
- 833 Guillén Fernández, and Bryan A Strange. 2019. “Propofol-Induced Deep Sedation

- 834 Reduces Emotional Episodic Memory Reconsolidation in Humans.” *Science Advances* 5
835 (3): eaav3801. <https://doi.org/10.1126/sciadv.aav3801>.
- 836 Gaskell, A. L., D. F. Hight, J. Winders, G. Tran, A. Defresne, V. Bonhomme, A. Raz, J. W.
837 Sleigh, and R. D. Sanders. 2017. “Frontal Alpha-Delta EEG Does Not Preclude
838 Volitional Response during Anaesthesia: Prospective Cohort Study of the Isolated
839 Forearm Technique.” *British Journal of Anaesthesia*, August.
840 <https://doi.org/10.1093/bja/aex170>.
- 841 Gemignani, Angelo, Danilo Menicucci, Marco Laurino, Andrea Piarulli, Francesca Mastorci,
842 Laura Sebastiani, and Paolo Allegrini. 2015. “Linking Sleep Slow Oscillations with
843 Consciousness Theories: New Vistas on Slow Wave Sleep Unconsciousness.” *Archives
844 Italiennes de Biologie* 153 (2–3): 135–43. <https://doi.org/10.4449/aib.v153i2-3.4041>.
- 845 Gil, Ziv, Barry W Connors, and Yael Amitai. 1997. “Differential Regulation of Neocortical
846 Synapses by Neuromodulators and Activity.” *Neuron* 19 (3): 679–86.
847 [https://doi.org/10.1016/S0896-6273\(00\)80380-3](https://doi.org/10.1016/S0896-6273(00)80380-3).
- 848 Gutiérrez, Rodrigo, Felipe Maldonado, Jose I. Egaña, and Antonello Penna. 2022.
849 “Electroencephalographic Alpha and Delta Oscillation Dynamics in Response to
850 Increasing Doses of Propofol.” *Journal of Neurosurgical Anesthesiology* 34 (1): 79–83.
851 <https://doi.org/10.1097/ANA.0000000000000733>.
- 852 Hage, Travis A, and Lawrence Salkoff. 2012. “Sodium-Activated Potassium Channels Are
853 Functionally Coupled to Persistent Sodium Currents.” *The Journal of Neuroscience* □:
854 *The Official Journal of the Society for Neuroscience*. 32 (8): 2714–21.
855 <https://doi.org/10.1523/JNEUROSCI.5088-11.2012>.

- 856 Hill, S. and Tononi, Giulio. 2004. "Modeling Sleep and Wakefulness in the Thalamocortical
857 System." *Journal of Neurophysiology* 93 (3): 1671–98.
858 <https://doi.org/10.1152/jn.00915.2004>.
- 859 Hsieh, C Y, S J Cruikshank, and R Metherate. 2000. "Differential Modulation of Auditory
860 Thalamocortical and Intracortical Synaptic Transmission by Cholinergic Agonist." *Brain*
861 *Res.* 880 (1–2): 51–64.
- 862 Hudetz, Anthony G., and George A. Mashour. 2016. "Disconnecting Consciousness: Is There a
863 Common Anesthetic End Point?" *Anesthesia & Analgesia* 123 (5): 1228–40.
864 <https://doi.org/10.1213/ANE.0000000000001353>.
- 865 Kikuchi, T, Y Wang, K Sato, and F Okumura. 1998. "In Vivo Effects of Propofol on
866 Acetylcholine Release from the Frontal Cortex, Hippocampus and Striatum Studied by
867 Intracerebral Microdialysis in Freely Moving Rats." *British Journal of Anaesthesia* 80
868 (5): 644–48. <https://doi.org/10.1093/bja/80.5.644>.
- 869 Krishnan, Giri P., Sylvain Chauvette, Isaac Shamie, Sara Soltani, Igor Timofeev, Sydney S.
870 Cash, Eric Halgren, and Maxim Bazhenov. 2016. "Cellular and Neurochemical Basis of
871 Sleep Stages in the Thalamocortical Network." *eLife* 5: e18607.
872 <https://doi.org/10.7554/eLife.18607>.
- 873 Krom, Aaron J., Amit Marmelshtein, Hagar Gelbard-Sagiv, Ariel Tankus, Hanna Hayat, Daniel
874 Hayat, Idit Matot, et al. 2020. "Anesthesia-Induced Loss of Consciousness Disrupts
875 Auditory Responses beyond Primary Cortex." *Proceedings of the National Academy of
876 Sciences*, May. <https://doi.org/10.1073/pnas.1917251117>.

- 877 Kruglikov, Illya, and Bernardo Rudy. 2008. “Perisomatic GABA Release and Thalamocortical
878 Integration onto Neocortical Excitatory Cells Are Regulated by Neuromodulators.”
879 *Neuron* 58 (6): 911–24. <https://doi.org/10.1016/j.neuron.2008.04.024>.
- 880 Kuo, Min-Ching, and Hans C. Dringenberg. 2008. “Histamine Facilitates in Vivo
881 Thalamocortical Long-Term Potentiation in the Mature Visual Cortex of Anesthetized
882 Rats.” *European Journal of Neuroscience* 27 (7): 1731–38.
883 <https://doi.org/10.1111/j.1460-9568.2008.06164.x>.
- 884 Lee, Minji, Robert D. Sanders, Seul-Ki Yeom, Dong-Ok Won, Kwang-Suk Seo, Hyun Jeong
885 Kim, Giulio Tononi, and Seong-Whan Lee. 2017. “Network Properties in Transitions of
886 Consciousness during Propofol-Induced Sedation.” *Scientific Reports* 7 (1): 16791.
887 <https://doi.org/10.1038/s41598-017-15082-5>.
- 888 Luo, Tian-Yuan, Shuang Cai, Zai-Xun Qin, Shao-Cheng Yang, Yue Shu, Cheng-Xi Liu, Yu
889 Zhang, et al. 2020. “Basal Forebrain Cholinergic Activity Modulates Isoflurane and
890 Propofol Anesthesia.” *Frontiers in Neuroscience* 14: 1086.
891 <https://doi.org/10.3389/fnins.2020.559077>.
- 892 Lytton, W. W., A. Destexhe, and T. J. Sejnowski. 1996. “Control of Slow Oscillations in the
893 Thalamocortical Neuron: A Computer Model.” *The Journal of Neuroscience* □ : The
894 Official Journal of the Society for Neuroscience. 70 (3): 673–84.
895 [https://doi.org/10.1016/S0306-4522\(96\)83006-5](https://doi.org/10.1016/S0306-4522(96)83006-5).
- 896 Malekmohammadi, Mahsa, Collin M. Price, Andrew E. Hudson, Jasmine A. T. DiCesare, and
897 Nader Pouratian. 2019. “Propofol-Induced Loss of Consciousness Is Associated with a
898 Decrease in Thalamocortical Connectivity in Humans.” *Brain*.
899 <https://doi.org/10.1093/brain/awz169>.

- 900 McCarthy, Michelle M., Emery N. Brown, and Nancy Kopell. 2008. "Potential Network
901 Mechanisms Mediating Electroencephalographic Beta Rhythm Changes during Propofol-
902 Induced Paradoxical Excitation." *The Journal of Neuroscience* □: The Official Journal of
903 the Society for Neuroscience. 28 (50): 13488–504.
904 <https://doi.org/10.1523/JNEUROSCI.3536-08.2008>.
- 905 McCormick, David A. 1992. "Neurotransmitter Actions in the Thalamus and Cerebral Cortex
906 and Their Role in Neuromodulation of Thalamocortical Activity." *Progress in
907 Neurobiology* 39 (4): 337–88. [https://doi.org/10.1016/0301-0082\(92\)90012-4](https://doi.org/10.1016/0301-0082(92)90012-4).
- 908 Meuret, P., S. B. Backman, V. Bonhomme, G. Plourde, and P. Fiset. 2000. "Physostigmine
909 Reverses Propofol-Induced Unconsciousness and Attenuation of the Auditory Steady
910 State Response and Bispectral Index in Human Volunteers." *Anesthesiology* 93 (3): 708–
911 17.
- 912 Mhuircheartaigh, Róisín Ní, Catherine Warnaby, Richard Rogers, Saad Jbabdi, and Irene Tracey.
913 2013. "Slow-Wave Activity Saturation and Thalamocortical Isolation during Propofol
914 Anesthesia in Humans." *Science Translational Medicine* 5 (208): 208ra148-208ra148.
- 915 Minert, Anne, Mark Baron, and Marshall Devor. 2020. "Reduced Sensitivity to Anesthetic
916 Agents upon Lesioning the Mesopontine Tegmental Anesthesia Area in Rats Depends on
917 Anesthetic Type." *Anesthesiology* 132 (3): 535–50.
918 <https://doi.org/10.1097/ALN.0000000000003087>.
- 919 Minert, Anne, Shai-Lee Yatziv, and Marshall Devor. 2017. "Location of the Mesopontine
920 Neurons Responsible for Maintenance of Anesthetic Loss of Consciousness." *Journal of
921 Neuroscience* 37 (38): 9320–31. <https://doi.org/10.1523/JNEUROSCI.0544-17.2017>.

- 922 Moody, Olivia A., Edlyn R. Zhang, Kathleen F. Vincent, Risako Kato, Eric D. Melonakos,
923 Christa J. Nehs, and Ken Solt. 2021. “The Neural Circuits Underlying General
924 Anesthesia and Sleep.” *Anesthesia & Analgesia* 132 (5): 1254–64.
925 <https://doi.org/10.1213/ANE.0000000000005361>.
- 926 Morrison, John H., and Mark G. Baxter. 2012. “The Aging Cortical Synapse: Hallmarks and
927 Implications for Cognitive Decline.” *Nature Reviews Neuroscience* 13 (4): 240–50.
928 <https://doi.org/10.1038/nrn3200>.
- 929 Muindi, Fanuel, Jonathan D. Kenny, Norman E. Taylor, Ken Solt, Matthew A. Wilson, Emery N.
930 Brown, and Christa J. Van Dort. 2016. “Electrical Stimulation of the Parabrachial
931 Nucleus Induces Reanimation from Isoflurane General Anesthesia.” *Behavioural Brain
932 Research* 306 (June): 20–25. <https://doi.org/10.1016/j.bbr.2016.03.021>.
- 933 Mukamel, E. A., E. Pirondini, B. Babadi, K. F. K. Wong, E. T. Pierce, P. G. Harrell, J. L. Walsh,
934 et al. 2014. “A Transition in Brain State during Propofol-Induced Unconsciousness.” *The
935 Journal of Neuroscience* □: The Official Journal of the Society for Neuroscience. 34 (3):
936 839–45. <https://doi.org/10.1523/JNEUROSCI.5813-12.2014>.
- 937 Nemoto, Chiaki, Masahiro Murakawa, Takahiro Hakozaki, Tuyoshi Imaizumi, Tuyoshi Isosu,
938 and Shinju Obara. 2013. “Effects of Dexmedetomidine, Midazolam, and Propofol on
939 Acetylcholine Release in the Rat Cerebral Cortex in Vivo.” *Journal of Anesthesia* 27 (5):
940 771–74. <https://doi.org/10.1007/s00540-013-1589-5>.
- 941 Neske, Garrett T. 2016. “The Slow Oscillation in Cortical and Thalamic Networks: Mechanisms
942 and Functions.” *Frontiers in Neural Circuits* 9 (January).
943 <https://doi.org/10.3389/fncir.2015.00088>.

- 944 Nunez, Paul L., and Ramesh Srinivasan. 2006. *Electric Fields of the Brain: The Neurophysics of*
945 *EEG*. 2nd ed. Oxford□; New York: Oxford University Press.
- 946 Oldford, E, and M. A Castro-Alamancos. 2003. “Input-Specific Effects of Acetylcholine on
947 Sensory and Intracortical Evoked Responses in the ‘Barrel Cortex’ in Vivo.”
948 *Neuroscience* 117 (3): 769–78. [https://doi.org/10.1016/S0306-4522\(02\)00663-2](https://doi.org/10.1016/S0306-4522(02)00663-2).
- 949 Onslow, Angela C.E., Rafal Bogacz, and Matthew W. Jones. 2011. “Quantifying Phase–
950 Amplitude Coupling in Neuronal Network Oscillations.” *Progress in Biophysics and*
951 *Molecular Biology* 105 (1–2): 49–57. <https://doi.org/10.1016/j.pbiomolbio.2010.09.007>.
- 952 Pal, Dinesh, and George A. Mashour. 2021. “Consciousness, Anesthesia, and Acetylcholine.”
953 *Anesthesiology* 134 (4): 515–17. <https://doi.org/10.1097/ALN.0000000000003696>.
- 954 Palva, Satu, and J. Matias Palva. 2007. “New Vistas for α -Frequency Band Oscillations.” *Trends*
955 *in Neurosciences* 30 (4): 150–58. <https://doi.org/10.1016/j.tins.2007.02.001>.
- 956 Penagos, Hector, Carmen Varela, and Matthew A Wilson. 2017. “Oscillations, Neural
957 Computations and Learning during Wake and Sleep.” *Current Opinion in Neurobiology*
958 44 (June): 193–201. <https://doi.org/10.1016/j.conb.2017.05.009>.
- 959 Peters, Alan. 2002. “Structural Changes That Occur during Normal Aging of Primate Cerebral
960 Hemispheres.” *Neuroscience and Biobehavioral Reviews* 26 (7): 733–41.
961 [https://doi.org/10.1016/S0149-7634\(02\)00060-X](https://doi.org/10.1016/S0149-7634(02)00060-X).
- 962 Purdon, P. L., K. J. Pavone, O. Akeju, A. C. Smith, A. L. Sampson, J. Lee, D. W. Zhou, K. Solt,
963 and E. N. Brown. 2015. “The Ageing Brain: Age-Dependent Changes in the
964 Electroencephalogram during Propofol and Sevoflurane General Anaesthesia.” *British*
965 *Journal of Anaesthesia* 115 (Suppl 1): i46–57. <https://doi.org/10.1093/bja/aev213>.

- 966 Purdon, P. L., E. T. Pierce, E. A. Mukamel, M. J. Prerau, J. L. Walsh, K. F. K. Wong, A. F.
967 Salazar-Gomez, et al. 2013. “Electroencephalogram Signatures of Loss and Recovery of
968 Consciousness from Propofol.” *Proceedings of the National Academy of Sciences of the
969 United States of America* 110 (12): E1142–51. <https://doi.org/10.1073/pnas.1221180110>.
970 Quick, Michael W., and Robin A. J. Lester. 2002. “Desensitization of Neuronal Nicotinic
971 Receptors.” *Journal of Neurobiology* 53 (4): 457–78. <https://doi.org/10.1002/neu.10109>.
972 Redinbaugh, Michelle J., Jessica M. Phillips, Niranjan A. Kambi, Sounak Mohanta, Samantha
973 Andryk, Gaven L. Dooley, Mohsen Afraziabi, Aeyal Raz, and Yuri B. Saalmann. 2020.
974 “Thalamus Modulates Consciousness via Layer-Specific Control of Cortex.” *Neuron* 106
975 (1): 66-75.e12. <https://doi.org/10.1016/j.neuron.2020.01.005>.
976 Sanchez-Vives, Maria V., and David A. McCormick. 2000. “Cellular and Network Mechanisms
977 of Rhythmic Recurrent Activity in Neocortex.” *Nature Neuroscience* 3 (10): 1027–34.
978 Sanchez-Vives, Maria V., Lionel G. Nowak, and David A. McCormick. 2000. “Cellular
979 Mechanisms of Long-Lasting Adaptation in Visual Cortical Neurons In Vitro.” *The
980 Journal of Neuroscience*: The Official Journal of the Society for Neuroscience. 20 (11):
981 4286–99. <https://doi.org/10.1523/JNEUROSCI.20-11-04286.2000>.
982 Schwindt, P C, W J Spain, and W E Crill. 1989. “Long-Lasting Reduction of Excitability by a
983 Sodium-Dependent Potassium Current in Cat Neocortical Neurons.” *Journal of
984 Neurophysiology* 61 (2): 233–44. <https://doi.org/10.1152/jn.1989.61.2.233>.
985 Sherfey, Jason S., Austin E. Soplat, Salva Ardid, Erik A. Roberts, David A. Stanley, Benjamin
986 R. Pittman-Polletta, and Nancy J. Kopell. 2018. “DynaSim: A MATLAB Toolbox for
987 Neural Modeling and Simulation.” *Frontiers in Neuroinformatics* 12.
988 <https://doi.org/10.3389/fninf.2018.00010>.

- 989 Soplata, Austin E. 2022a. *Dynasim Fork for Soplata 2022*.
990 https://github.com/asoplata/DynaSim/tree/coupling_addition.
991 ———. 2022b. *Full Soplata 2022 Code*. <https://github.com/asoplata/soplata-2022-thalcort-code>.
992 ———. 2022c. *Mechanism Code for Soplata 2022 Model*. MATLAB.
993 https://github.com/asoplata/dynasim-extended-benita-model.
994 Soplata, Austin E., Michelle M. McCarthy, Jason Sherfey, Shane Lee, Patrick L. Purdon, Emery
995 N. Brown, and Nancy Kopell. 2017. “Thalamocortical Control of Propofol Phase-
996 Amplitude Coupling.” *PLoS Computational Biology* 13 (12): e1005879.
997 https://doi.org/10.1371/journal.pcbi.1005879.
998 Stephen, Emily P., Gladia C. Hotan, Eric T. Pierce, P. Grace Harrell, John L. Walsh, Emery N.
999 Brown, and Patrick L. Purdon. 2020. “Broadband Slow-Wave Modulation in Posterior
1000 and Anterior Cortex Tracks Distinct States of Propofol-Induced Unconsciousness.”
1001 *Scientific Reports* 10 (1): 13701. <https://doi.org/10.1038/s41598-020-68756-y>.
1002 Stickgold, Robert. 2005. “Sleep-Dependent Memory Consolidation.” *Nature* 437 (7063): 1272–
1003 78. <https://doi.org/10.1038/nature04286>.
1004 Taxidis, Jiannis, Kenji Mizuseki, Robert Mason, and Markus R. Owen. 2013. “Influence of Slow
1005 Oscillation on Hippocampal Activity and Ripples through Cortico-Hippocampal Synaptic
1006 Interactions, Analyzed by a Cortical-CA3-CA1 Network Model.” *Frontiers in*
1007 *Computational Neuroscience* 7. <https://doi.org/10.3389/fncom.2013.00003>.
1008 Timofeev, I., F. Grenier, M. Bazhenov, T. J. Sejnowski, and M. Steriade. 2000. “Origin of Slow
1009 Cortical Oscillations in Deafferented Cortical Slabs.” *Cerebral Cortex (New York, N.Y.: 1991)* 10 (12): 1185–99. <https://doi.org/10.1093/cercor/10.12.1185>.

- 1011 Tinker, John H., Frank W. Sharbrough, and John D. Michenfelder. 1977. “Anterior Shift of the
1012 Dominant EEG Rhythm during Anesthesia in the Java Monkey: Correlation with
1013 Anesthetic Potency.” *Anesthesiology*.
- 1014 Tort, A. B. L., R. Komorowski, H. Eichenbaum, and N. Kopell. 2010. “Measuring Phase-
1015 Amplitude Coupling Between Neuronal Oscillations of Different Frequencies.” *Journal*
1016 *of Neurophysiology* 104 (2): 1195–1210. <https://doi.org/10.1152/jn.00106.2010>.
- 1017 Traub, Roger D, Diego Contreras, Mark O Cunningham, Hilary Murray, Fiona E N LeBeau,
1018 Anita Roopun, Andrea Bibbig, W Bryan Wilent, Michael J Higley, and Miles A
1019 Whittington. 2005. “Single-Column Thalamocortical Network Model Exhibiting Gamma
1020 Oscillations, Sleep Spindles, and Epileptogenic Bursts.” *J. Neurophysiol.* 93 (4): 2194–
1021 2232.
- 1022 Vijayan, S., S. Ching, P. L. Purdon, E. N. Brown, and N. J. Kopell. 2013. “Thalamocortical
1023 Mechanisms for the Anteriorization of Alpha Rhythms during Propofol-Induced
1024 Unconsciousness.” *The Journal of Neuroscience* □: The Official Journal of the Society for
1025 Neuroscience. 33 (27): 11070–75. <https://doi.org/10.1523/JNEUROSCI.5670-12.2013>.
- 1026 Vlasov, Ksenia, JunZhu Pei, Christa J. Nehs, Jennifer A. Guidera, Edlyn R. Zhang, Jonathan D.
1027 Kenny, Timothy T. Houle, Gary J. Brenner, Norman E. Taylor, and Ken Solt. 2021.
1028 “Activation of GABAergic Neurons in the Rostromedial Tegmental Nucleus and Other
1029 Brainstem Regions Promotes Sedation and Facilitates Sevoflurane Anesthesia in Mice.”
1030 *Anesthesia & Analgesia* 132 (4): e50. <https://doi.org/10.1213/ANE.0000000000005387>.
- 1031 Ying, Shui-Wang, Syed Y. Abbas, Neil L. Harrison, and Peter A. Goldstein. 2006. “Propofol
1032 Block of I_h Contributes to the Suppression of Neuronal Excitability and Rhythmic Burst
1033 Firing in Thalamocortical Neurons: Propofol Inhibition of Thalamic I_h .” *The European*

1034 *Journal of Neuroscience* 23 (2): 465–80. <https://doi.org/10.1111/j.1460->

1035 9568.2005.04587.x.

1036

Figure Captions

1037 **Figure 1: EEG alpha and slow phase-amplitude coupling during human propofol anesthesia.**

1038 (A) Frontal EEG recorded at different propofol doses in human patients (data from (Purdon et al. 2013)).
1039 (B) EEG data from A but filtered at alpha (red) and slow (green) frequencies. (C) Stepwise changes in
1040 propofol dose throughout the experiment. (D) Comodulogram of alpha frequency amplitude coupling to
1041 slow frequency phase of EEG activity in A. (D) Spectrogram of EEG activity in A. Red vertical line
1042 marks the time of loss of consciousness.

1043

1044 **Figure 2: The simulated thalamocortical network is capable of relay-mode firing.**

1045 (A) Illustration of thalamocortical Hodgkin-Huxley network model used for all simulations; for details,
1046 see Methods. (B) Rastergrams of each cell/compartment in a relay-mode state, in which each black line
1047 represents a spike by each cell/compartment.

1048

1049 **Figure 3: Applying direct propofol effects to the thalamocortical network do not enable propofol**
1050 **alpha or slow oscillations.**

1051 (A) Rastergrams of each cell/compartment spikes in simulation with direct propofol effects applied. Note
1052 the lack of slow or alpha oscillation by excitatory cells throughout the simulation, and that the TC cell
1053 population is quiescent. This represents only spiking information, not voltage activity. (B) Voltage trace
1054 of a single TC cell. (C) Steady-state curves across voltage for both the “m” activation gate and “h”
1055 inactivation gate of the TC cell T-current, with shaded region indicating activation region of “h” gate.

1056

1057 **Figure 4: Simulating both direct and indirect propofol effects enables the thalamocortical network**
1058 **to exhibit both slow and alpha oscillations.**

1059 Rastergram of a simulation including both direct and indirect propofol effects. Each black line represents
1060 a spike by each cell/compartment. Blue highlight indicates time periods of the first distinct dynamic state
1061 of the network, and orange highlight indicates the second dynamic state of the network.

1062

1063 **Figure 5: Different slow cycles of a low-dose propofol simulation display either trough-max or**
1064 **peak-max alpha-slow PAC.**

1065 (A) Representative voltage traces of each cell/compartment during a time period of the simulation
1066 expressing trough-max. (B) Representative voltage traces of each cell/compartment type across the low-
1067 dose propofol simulation, with time periods of either coupling regime highlighted; blue is trough-max,
1068 and orange is peak-max. This is the same simulation as that of Figure 4. (C) Representative voltage traces
1069 of each cell/compartment during a time period of the simulation expressing peak-max. (D) Rastergram of
1070 all spiking activity during the indicated trough-max time range of the simulation. (E) Rastergram of all
1071 spiking activity across the simulation, with coupling regimes highlighted. (F) Rastergram of all spiking
1072 activity during the indicated peak-max time range of the simulation.

1073

1074 **Figure 6: During a peak-max time period, both sets of synaptic currents are high only near cortical**
1075 **UP states.**

1076 (A) Example voltage traces of each cell/compartment type across the low-dose propofol simulation. The
1077 red box indicates which peak-max time window is explored in the rest of the figure. (B) Example voltage
1078 trace of receiving PYdr compartment of a TC→PY synapse. (C) Example voltage trace of a source TC
1079 cell of a TC→PY synapse. (D) Total TC→PY synaptic AMPA currents. (E) Example voltage trace of
1080 receiving PYdr compartment of a PY→PY synapse. (F) Example voltage trace of a source PYso
1081 compartment of a PY→PY synapse. (G) Total PY→PY synaptic AMPA currents.

1082 **Figure 7: During peak-max time periods in a low-dose propofol simulation, both TC→PY and**
1083 **PY→PY synaptic currents are high during the alpha bursting and cortical UP states, enabling**
1084 **cooperation in the final signal.**

1085 (A) TC→PY synaptic current during the peak-max time period from Figure 6. (B) PY→PY synaptic
1086 current during the peak-max time period from Figure 6. (C) Combination of TC→PY and PY→PY
1087 synaptic currents. (D) slow-phase alpha-amplitude comodulogram of combined synaptic currents for the
1088 entire simulation.

1089 **Figure 8: During trough-max, TC→PY synapses produce more current in the trough, while weaker**
1090 **PY→PY synapses produced peak-max currents.**

1091 (A) Example voltage traces of each cell/compartment type across the low-dose propofol simulation. The
1092 red box indicates which trough-max time period is explored in the rest of the figure. (B) Example voltage
1093 trace of a receiving PYdr compartment of a TC→PY synapse. (C) Example voltage trace of a source TC
1094 cell of a TC→PY synapse. (D) Total TC→PY synaptic AMPA currents. (E) Zoom of D, showing the
1095 slow-phase modulation of the alpha oscillation amplitude across TC→PY synapses. Dashed lines indicate
1096 where this synaptic current is maximal. (F) Example voltage trace of a receiving PYdr compartment of a
1097 PY→PY synapse. (G) Example voltage trace of a source PYso compartment of a PY→PY synapse. (H)
1098 Total PY→PY synaptic AMPA currents. Note the large difference in amplitude between TC→PY and
1099 PY→PY synapses.

1100 **Figure 9: During trough-max, TC→PY synaptic currents dominate PY→PY synaptic currents.**

1101 (A) TC→PY synaptic current during trough-max time period from Figure 8. (B) PY→PY synaptic
1102 current during trough-max time period from Figure 8. Note the much smaller amplitude than A. (C)
1103 Combination of TC→PY and PY→PY synaptic currents, which is almost the same as A. (D) slow-phase

1104 alpha-amplitude comodulogram of combined synaptic currents for the entire simulation, with
1105 corresponding trough-max time period indicated.

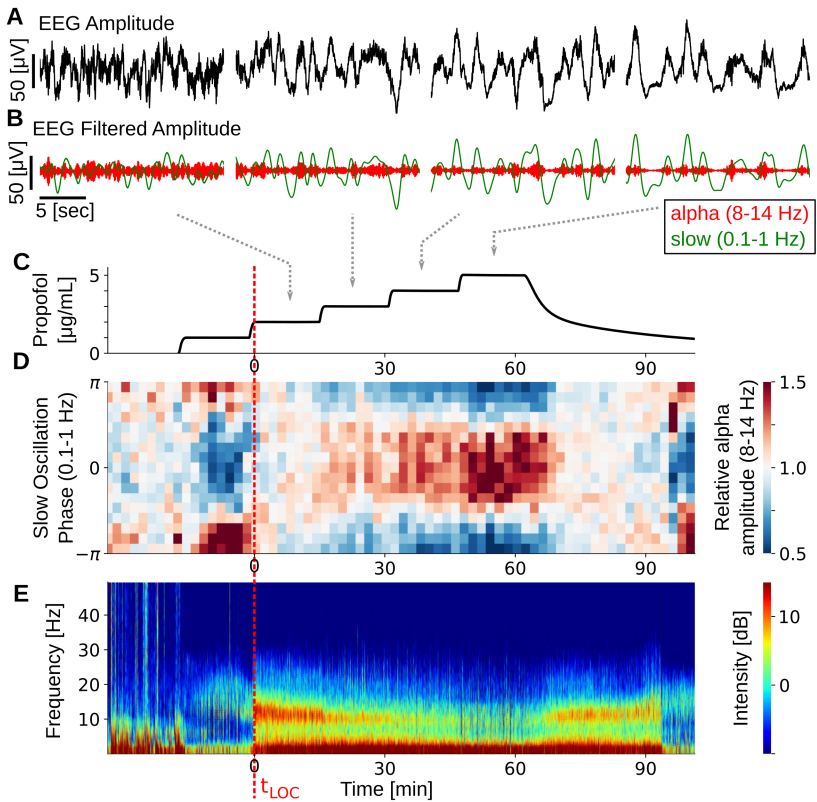
1106 **Figure 10: Cortical pyramidal slow oscillation synchronization is associated with the degree of**
1107 **network trough-max PAC versus peak-max conditions.**

1108 Trough-max: (A) Example trace of total TC→PYdr AMPA current, showing alpha-slow trough-max. (B)
1109 Rastergram of PYdr compartment spikes and TC cell spikes, where each black pixel represents a spike.
1110 Note the weakly synchronous slow component in the cortex and persistent propofol alpha in the thalamus.
1111 PYdr and PYso activity for any one cell is virtually identical. (C) Example trace of total corticothalamic
1112 PYso→TC AMPA current, showing UP-grouped firing. Peak-max PAC: (D) Example trace of total
1113 TC→PYdr AMPA current, showing alpha-slow peak-max. (E) Rastergram of PYdr compartment spikes
1114 and TC cell spikes. Note the strong synchronicity of UP/DOWN states and thalamic alpha oscillations
1115 only near PYdr UP states. (F) Example trace of total corticothalamic PYso→TC AMPA current, showing
1116 slow-synchronous corticothalamic activity that is grouped more strongly.

1117

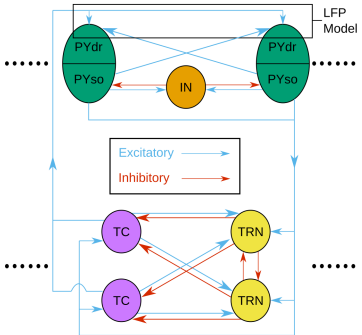
1118 **Figure 11: Increasing indirect effects of propofol shifts the low-dose, trough-max preferring**
1119 **network to a high-dose, peak-max preferring one.**

1120 Graphic illustrating different inputs and output results of each simulation class. All simulations show
1121 different trough-max and peak-max during different slow cycles, but the proportion of trough-max versus
1122 peak-max is variable across simulations.

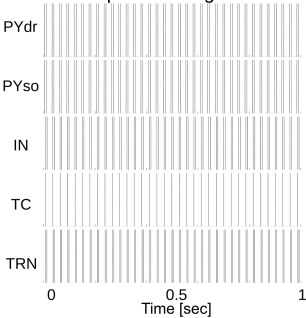


A

Simulated Circuit Model Network

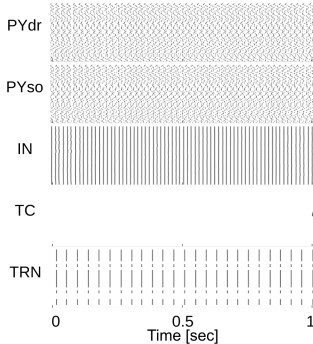
**B**

Relay-mode Spike Rastergrams

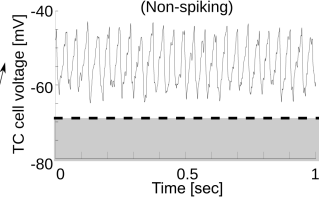


A

Propofol (Direct Effects Only)
Spike Rastergrams

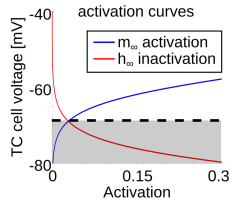
**B**

Single TC Cell Voltage Trace
(Non-spiking)

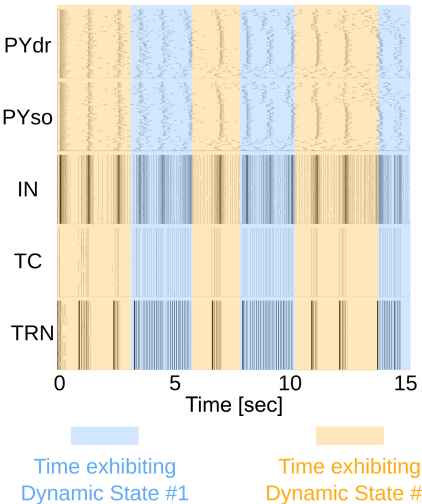
**C**

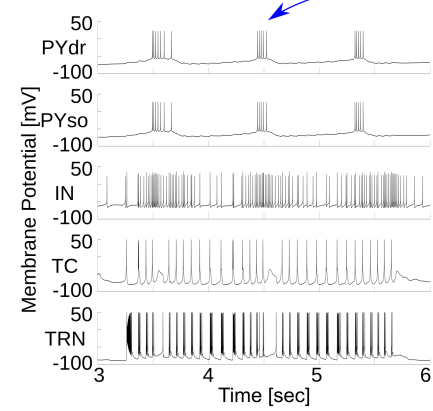
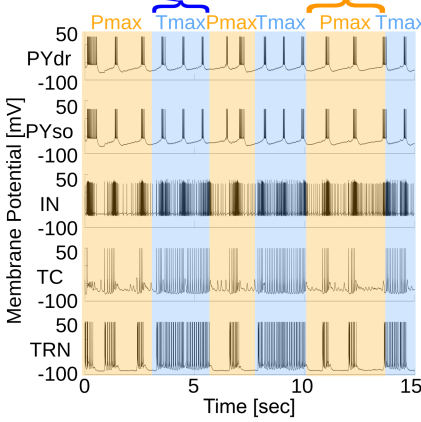
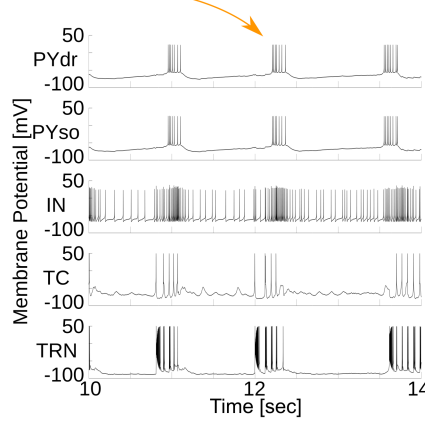
TC cell T-current activation curves

— m_{∞} activation
— h_{∞} inactivation



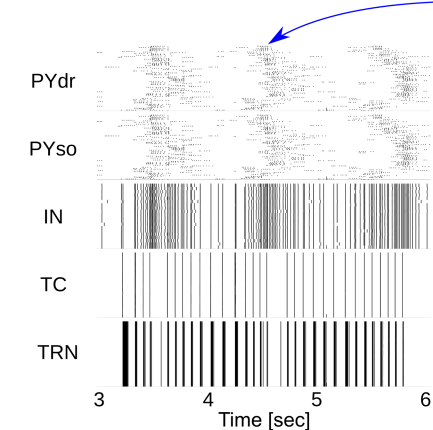
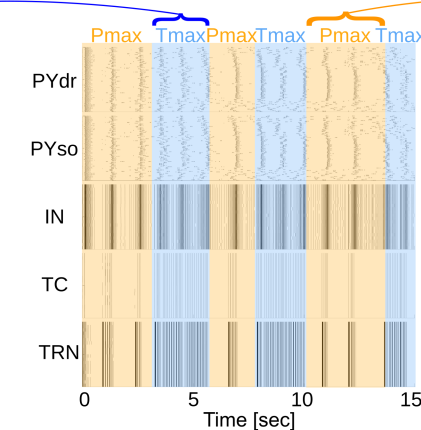
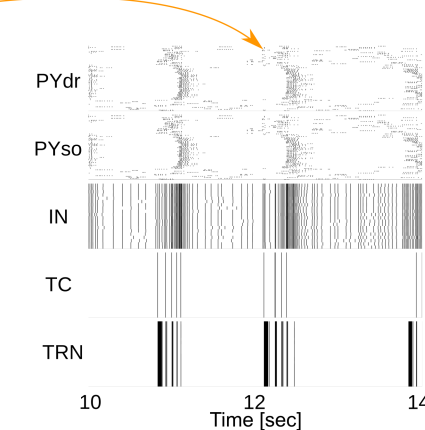
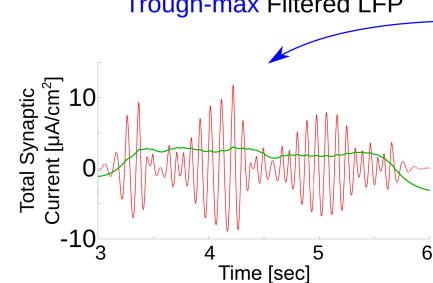
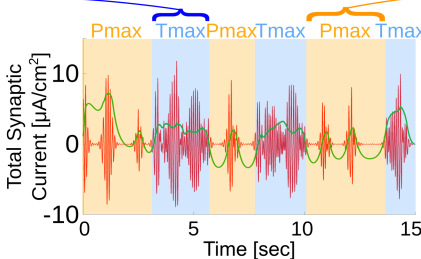
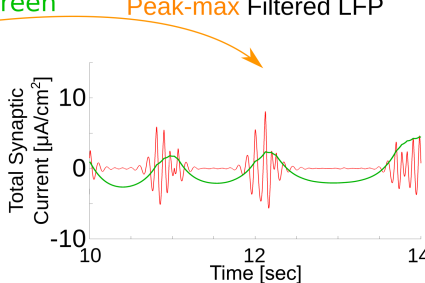
Simulation Spike Rastergram (Direct and Indirect Propofol Effects)



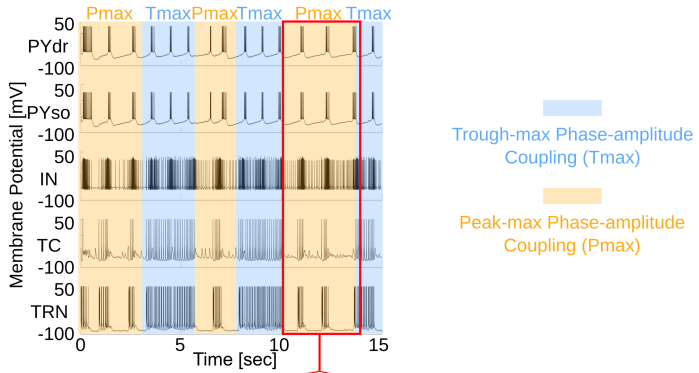
A Trough-max Voltage Traces**B Single Voltage Traces****C Peak-max Voltage Traces**

Trough-max Phase-amplitude Coupling (Tmax)

Peak-max Phase-amplitude Coupling (Pmax)

D Trough-max Spike Rastergram**E Spike Rastergram****F Peak-max Spike Rastergram****G Trough-max Filtered LFP****H Simulated total LFP signal
Filtered for alpha in red, slow in green****I Peak-max Filtered LFP**

A Propofol Single Voltage Traces



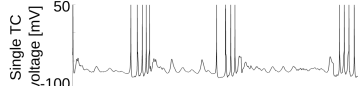
Thalamocortical TC → PY AMPA synapses
during Peak-max

Intracortical PY → PY AMPA synapses
during Peak-max

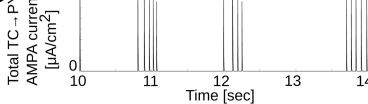
B Synaptic Current Traces



C Synaptic Current Traces



D Total TC → PY AMPA current



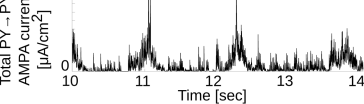
E Synaptic Current Traces



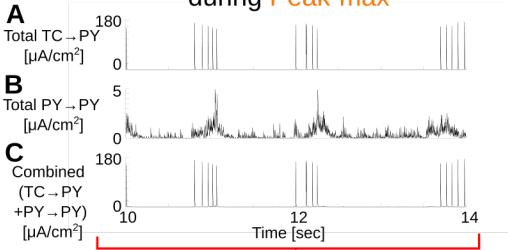
F Synaptic Current Traces



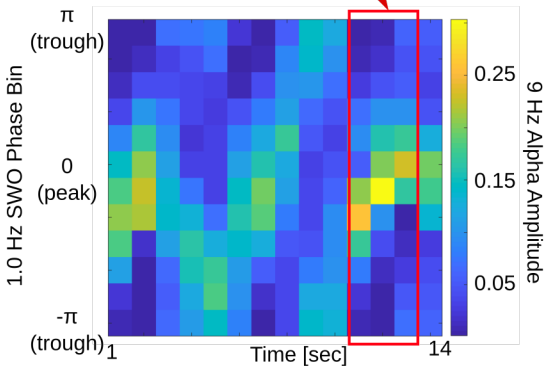
G Total PY → PY AMPA current

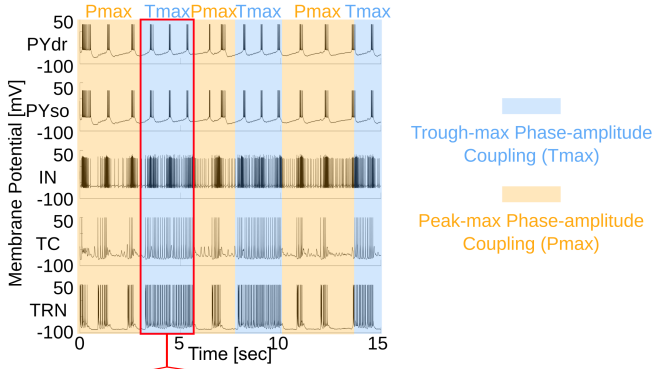


AMPAergic synaptic currents during Peak-max



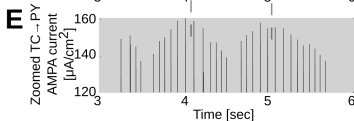
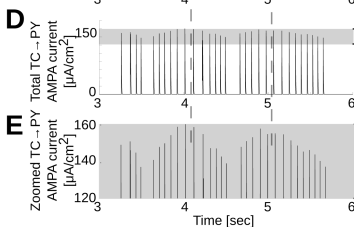
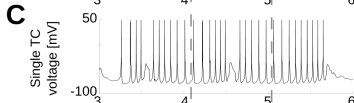
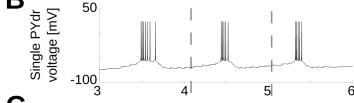
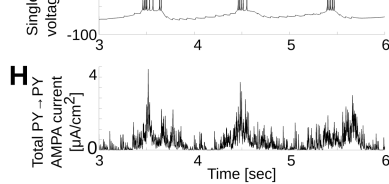
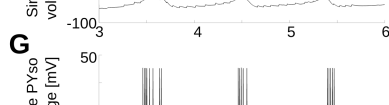
D Alpha-amplitude/SWO-phase
comodulogram of combined currents
during Peak-max



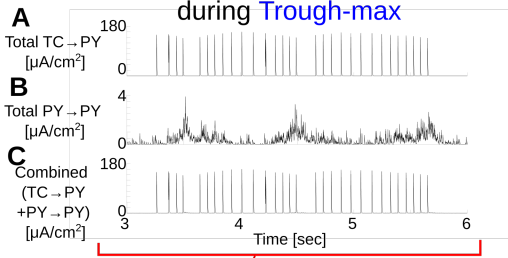
A Propofol Single Voltage Traces

Thalamocortical TC → PY AMPA synapses
during **Trough-max**

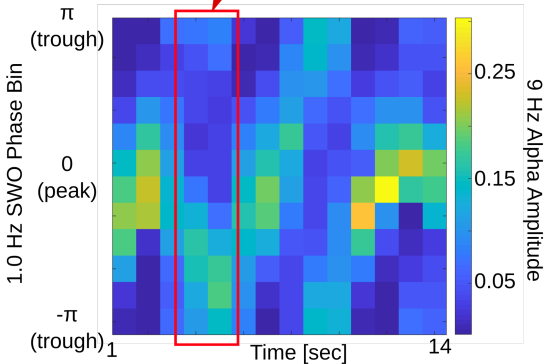
Intracortical PY → PY AMPA synapses
during **Trough-max**

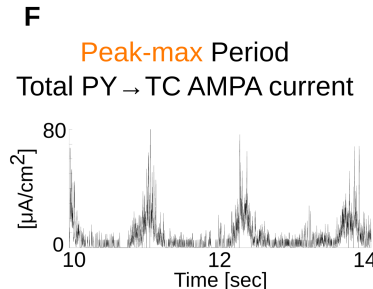
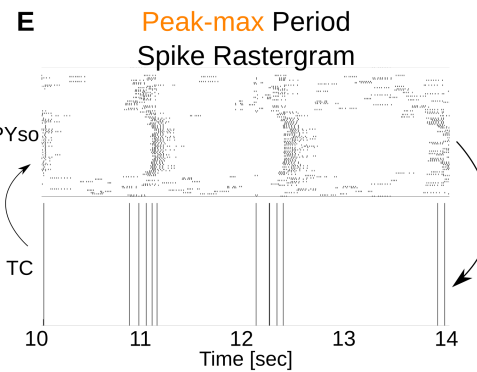
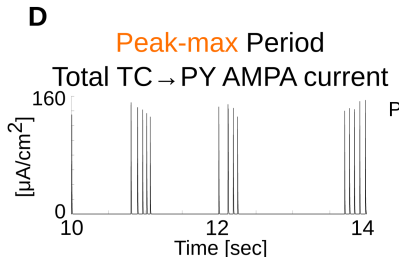
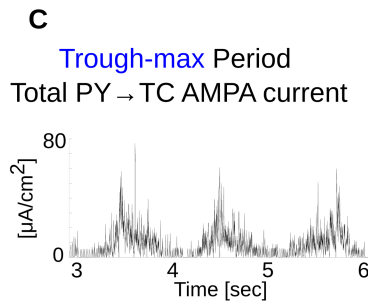
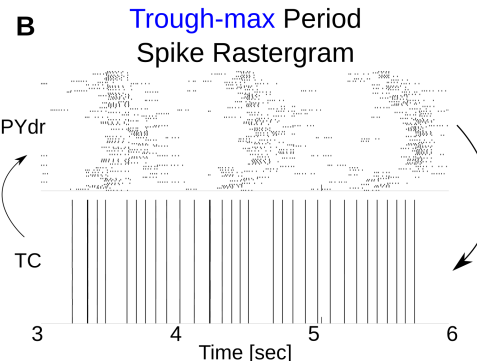
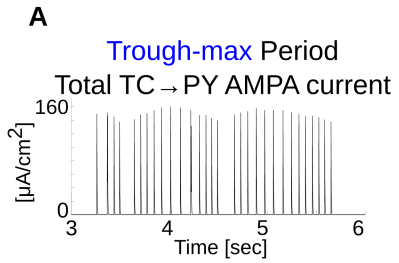
B Synaptic Current Traces**F Synaptic Current Traces**

AMPAergic synaptic currents during Trough-max



D Alpha-amplitude/SWO-phase
comodulogram of combined currents
during Trough-max





Breakdown of dose-specific simulation results

Input Parameters

↑ dose = ↓ ACh

Low-dose propofol

Direct effects:
TC $g_H \downarrow$
 $g_{GABA_A} \uparrow$
 $\tau_{GABA_A} \uparrow$

Indirect effects:
 $g_{KNa} \uparrow$
 $g_{AMPA:TC \rightarrow PY} \uparrow$
 $g_{AMPA:PY \rightarrow PY} \uparrow$

High-dose propofol

Direct effects:
TC $g_H \downarrow$
 $g_{GABA_A} \uparrow$
 $\tau_{GABA_A} \uparrow$

Indirect effects:
 $g_{KNa} \uparrow\uparrow$
 $g_{AMPA:TC \rightarrow PY} \uparrow\uparrow$
 $g_{AMPA:PY \rightarrow PY} \uparrow\uparrow$

53% chance
($\pm 20\%$)

47% chance
($\pm 20\%$)

27% chance
($\pm 13\%$)

73% chance
($\pm 13\%$)

Trough-max

Peak-max

Results

TC → PY synaptic currents exhibit
Trough-max

PY → PY synaptic currents exhibit
Peak-max
(weaker than TC → PY)

Both synaptic currents exhibit
Peak-max